Ecological Monographs, 64(3), 1994, pp. 287–313

MECHANICAL CONSEQUENCES OF SIZE IN WAVE-SWEPT ALGAE[1]

BRIAN GAYLORD[2]
Hopkins Marine Station of Stanford University, Pacific Grove, California 93950 USA

CAROL A. BLANCHETTE[2]
Department of Zoology, Oregon State University, Corvallis, Oregon 97331 USA

MARK W. DENNY[2]
Hopkins Marine Station of Stanford University, Pacific Grove, California 93950 USA

Abstract. The intertidal zone of wave-swept rocky shores is characterized by high velocities and exceedingly rapid accelerations. The resulting hydrodynamic forces (drag, lift, and the accelerational force) have been hypothesized both to set an upper limit to the size to which wave-swept organisms can grow and to establish an optimal size at which reproductive output is maximized. This proposition has been applied previously to intertidal animals that grow isometrically, in which case the accelerational force is the primary scaling factor that constrains size. In contrast, it has been thought that the size of wave-swept algae is limited by the interaction of drag alone with these plants' allometric pattern of growth.

Here we report on empirical measurements of drag and accelerational force in three common species of intertidal algae (*Gigartina leptorhynchos, Pelvetiopsis limitata,* and *Iridaea flaccida*). The drag coefficients for these species decrease with increased water velocity, as is typical for flexible organisms. For two of these species, this decline in drag coefficient is dramatic, leading to small drag forces with concomitant low drag-induced mortality at plant sizes near those observed in the field. However, all three species have surprisingly large inertia coefficients, suggesting that these plants experience large accelerational forces in surf-zone flows. Preliminary calculations show that these accelerational forces combine with drag to act as a size-dependent agent of mortality, constraining the size of these algae.

This study further models the interplay between size-dependent survivorship and reproductive ability to predict the size at which reproductive output peaks. This "optimal size" depends on the strength distribution and morphology of the algal species and on the flow regime characteristic of a particular site. This study shows that the optimal size predicted for *G. leptorhynchos,* calculated using velocities and accelerations typical of the moderately protected location where this species was collected, closely matches its observed mean size. Similarly, the predicted optimal sizes of *P. limitata* and *I. flaccida* at the exposed site where these plants were sampled also match their mean observed sizes. These data, although preliminary, suggest that mechanical factors (in particular the accelerational force) may be important in limiting the size of intertidal macroalgae and that attention solely to biological constraints may be inappropriate.

Key words: accelerational force; added mass; disturbance; drag; inertia coefficient; intertidal macroalgae; mechanical limits; optimal size; seaweed; size constraints; wave exposure; wave forces.

INTRODUCTION

The intertidal zone of wave-swept rocky shores is characterized by violent water motion. Velocities as high as 14–16 m/s have been measured (Jones and Demetropoulos 1968, Denny et al. 1985), accompanied by accelerations in excess of 400 m/s^2 (Denny et al. 1985). These flows have many biological consequences. For example, Leigh et al. (1987) have shown that primary productivity on wave-swept shores is extraordinarily high, a fact they attribute to the increased nutrient supply and constant rearrangement of fronds associated with wave-induced water motion. The shoreward surge of water in the surf zone also acts as a major contributing factor in setting the species-specific vertical limits to habitation on the shore (Stephenson and Stephenson 1949). The more violent the flow, the higher on the shore water is tossed, and the higher organisms may reliably survive. Wave-induced flows also place substantial hydrodynamic forces on intertidal plants and animals (e.g., Koehl 1977*a, b, c,* 1984, 1986, Denny et al. 1985, Denny 1988), with a variety of effects. For example, wave-induced forces

[1] Manuscript received 31 October 1992; accepted 29 July 1993.

[2] The authors are pleased to note that this study was a true three-way collaboration. Order of authorship was therefore determined by a coin toss.

may be a controlling factor in the rate of disturbance in species that dominate the competition for space (e.g., Dayton 1971, Paine and Levin 1981, Sousa 1984, 1985) and can thereby influence the course of succession, and hence species richness, in intertidal communities.

Wave-induced hydrodynamic forces may also set mechanical limits to the size to which wave-swept animals can grow before the probability of being dislodged approaches certainty, and can potentially determine the size at which animals have a maximal reproductive output (Denny et al. 1985). The argument is as follows. Wave-swept organisms encounter forces associated both with the velocity of the water around them (lift and drag) and with the water's acceleration (the accelerational force). Lift and drag are proportional to a representative area of the organism, as is the force required for breakage or dislodgment (i.e., breaking force depends on cross-sectional area and adhesive failure on attachment area). Thus, if an organism maintains a constant shape and if its adhesive or material properties do not change as it grows, the risk of death due to breakage/dislodgment from lift or drag remains independent of size. The accelerational force, however, varies in proportion to the volume of the organism, and therefore increases faster with a given increment in size than does the organism's ability to remain attached to the substratum. Large organisms thus have a higher risk of breakage or dislodgment.

Denny et al. (1985) applied this argument to several intertidal animals with varying success. The observed maximal size of sea urchins, solitary mussels, and limpets appeared to fit predictions in that their observed maximal sizes were close to the optimal size (i.e., the size of maximal predicted reproductive output) calculated on the basis of hydrodynamic forces. Others, such as barnacles, were much smaller than the predicted optimal size, while results for a hydrocoral, *Millepora complanata,* were inconclusive.

Denny et al. (1985) made no attempt to apply their argument to wave-swept algae. Unlike the animals studied, intertidal macroalgae often do not grow isometrically, thereby violating one of the basic assumptions of their approach. Furthermore, because algae often have a flexible, blade-like structure, it was assumed that these plants would behave as flat plates aligned parallel to the direction of flow and would therefore experience a negligible accelerational force. Thus, any mechanical limits to size in wave-swept algae remained unexplored.

More recently, Carrington (1990) has shown that changes in shape of a macroalga as it grows can, in conjunction with drag, form a limit to the size of the plant. *Mastocarpus papillatus,* a high intertidal red alga, maintains a stipe with a cross-sectional area that remains essentially constant while the thallus (the primary source of drag) continues to increase in size during growth. For a given water velocity, there is thus a maximal size to which a *M. papillatus* thallus can grow before the ability of the stipe to resist drag is in all probability exceeded. Alternatively, there is a maximal water velocity that can be resisted by a thallus of a given size. For *M. papillatus* thalli of typical size (maximum projected area of 0.0007–0.001 m^2), this limiting water velocity is quite high (10–20 m/s), but within the range predicted for storm waves. Carrington's (1990) data suggest, therefore, that drag can constrain the size of plants of this species.

Carrington (1990) also demonstrated that the flexibility of *M. papillatus* allows it to reconfigure to a streamlined shape that reduces its coefficient of drag at high velocities, a behavior she found characteristic of several other intertidal macroalgae as well. While data for additional species tested in the present study also conform to this trend, we report that for some algae this reduction in drag coefficient is larger than that for *M. papillatus* and is sufficient to remove any practical limit to size set by the interaction of drag and the change in morphology during ontogeny. What, then, limits size in these species? Here we reexamine the possibility that the accelerational force (in conjunction with drag) may mechanically limit the size of a variety of wave-swept algae.

We propose that even in their streamlined configuration, algae tend to trap a substantial volume of slower moving water in and amongst their thalli, increasing the plant's effective volume and thus the accelerational force. Our preliminary calculations suggest that the risk of breakage associated with this force may constrain the size to which plants can grow while still retaining a reasonable probability of surviving to reproduce.

Theory

Hydrodynamic forces

Objects in unsteady flow (such as that of the surf zone) encounter three hydrodynamic forces: drag, lift, and the accelerational force. Drag, F_d, is typically described by the equation:

$$F_d = (1/2)C_d\rho A_c|u|u, \quad (1)$$

where C_d is the dimensionless drag coefficient, ρ is the mass density of the fluid, A_c is a characteristic area (usually the object's frontal area, its area projected onto a plane perpendicular to flow), and u is the velocity of the water relative to the object. See Table 1 for a brief description of all variables.

The magnitude of C_d is a function of the Reynolds number, Re, which represents the ratio of inertial to viscous forces in steady (time-independent) flow (Vogel 1981, Middleton and Southard 1984):

$$\mathrm{Re} = \rho ux/\mu. \quad (2)$$

In this equation x is a characteristic length of the object in the direction of flow and μ is the dynamic viscosity of the fluid.

In oscillatory flow, where the direction of fluid mo-

TABLE 1. Symbols used in the text.

Symbol	Units	Definitions
a	m/s^2	Acceleration
A	m^2	Maximum projected area of an alga
A_c	m^2	Characteristic area
A_{opt}	m^2	Optimal area (size) of an alga
C_a	...	Added mass coefficient
C_d	...	Drag coefficient
$C_{d,avg}$	...	Drag coefficient averaged over a cycle
C_l	...	Lift coefficient
C_m	...	Inertia coefficient
$C_{m,avg}$	...	Inertia coefficient averaged over a cycle
E	...	Vogel number
$f(t)$	...	Arbitrary periodic function
F	N	Total in-line force (drag plus accelerational force)
F_a	N	Accelerational force
$F_{a,max}$	N	Maximal accelerational force in a cycle
F_d	N	Drag
$F_{d,k}$	N	Drag at k^{th} sampling point in cycle
$F_{d,max}$	N	Predicted maximal drag on a wave-swept organism for a given period of exposure
F_k	N	Total in-line force at k^{th} sampling point in a cycle
F_l	N	Lift force
F_{max}	N	Maximum total in-line force in a cycle
H_m	m	Mean significant wave height
i	...	Numerical index
j	...	Breaking force rank
k	...	Sampling point through a cycle (0 to 31)
K	...	Period parameter (Keulegan–Carpenter number)
$M_{y,max}$	...	Ratio of predicted maximal wave height to mean significant wave height for a given time period
n	...	Fourier harmonic number
N	...	Total number of plants of each species tested for breaking strength
P	...	Probability
q	...	Number of sampling points used to define cycle
Re	...	Reynolds number
t	s	Time
T	s	Period
u	m/s	Velocity
u_k	m/s	Velocity at k^{th} sampling point in cycle
u_{max}	m/s	Maximum velocity in cycle
V	m^3	Volume
x	m	Characteristic length in the direction of flow
z_1-z_7	...	Constants
α	...	Weibull model parameter
α_n	...	Coefficient of n^{th} Fourier cosine harmonic
β	...	Weibull model parameter
β_n	...	Coefficient of n^{th} Fourier sine harmonic
ϵ	...	Weibull model parameter
μ	$N \cdot s \cdot m^{-2}$	Dynamic viscosity
ϕ	rad	Phase angle, $2\pi t/T$
Φ	rad	Angle between lines of lift and drag forces
ρ	kg/m^3	Mass density

tion reverses periodically, C_d may also vary with another dimensionless number, the period parameter (also called the Keulegan-Carpenter number), K, defined as:

$$K = u_{max}T/x, \quad (3)$$

where u_{max} is the maximum velocity in an oscillatory cycle, T is the period of the cycle, and x is again a characteristic length of the object. The period parameter provides a measure of how far the fluid travels in each direction relative to the size of the object.

For large K (>100), such as that associated with intertidal macroalgae and the water motion produced by waves, the fluid travels many times the length of the object during an oscillatory event, and flow patterns may approximate those in steady flow. At smaller period parameters, additional complexity may be introduced. For example, the drag coefficients of spheres and cylinders in harmonic flow at Reynolds numbers below $\approx 10^5$ can deviate substantially from steady flow values (Sarpkaya and Tuter 1974, Sarpkaya and Isaacson 1981). While this phenomenon is most noticeable for $K < 20$, it has been shown to occur for period parameters at least as large as 100 (Sarpkaya and Isaacson 1981). Thus, measurements of drag coefficients in steady flow cannot be uncritically extended to unsteady flow.

For flexible objects such as algae, calculations using Eq. 1 are complicated by the possibility that the area oriented perpendicular to flow can change. To avoid the problems inherent in measuring area as a function

of velocity, biologists typically use the organism's maximum projected area, A, as the characteristic area when calculating C_d, regardless of the plant's instantaneous orientation (e.g., Vogel 1981, 1989, Denny 1988, Carrington 1990). This convention is used here.

The second major force, lift (F_l), can be described in a similar fashion to drag:

$$F_l = (1/2)C_l\rho A_c u^2, \quad (4)$$

where the characteristic area in this case is typically taken to be the planform area (the area projected onto a plane parallel to the direction of flow) rather than the frontal area. C_l is the dimensionless lift coefficient, analogous to C_d. Lift acts perpendicular to the direction of flow and not necessarily upward against gravity.

Although lift can be substantial under certain conditions (e.g., Denny 1987*a*, 1989), it is probably not important for the flexible intertidal algae studied here. The combination of lift and drag on an algal thallus results in a net force directed at an angle Φ to the substratum. A consideration of the geometry of the situation shows that in steady flow $\tan \Phi = F_l/F_d$. Because the stipe is flexible, it becomes aligned with the net force on the thallus. Thus, the angle of the stipe in flow provides a crude estimate of the relative magnitudes of lift and drag. Our observations of intertidal algae in rapid flow suggest that Φ is typically near zero, indicating that lift is negligible relative to drag. Note that this method for estimating the relative magnitudes of lift and drag is unlikely to apply to situations with relatively low velocities (such as in flows characteristic of subtidal habitats) where the stiffness of the plant often cannot be neglected in comparison with hydrodynamic forces.

While both drag and lift can occur in steady flow, the third major force, the accelerational force (F_a), appears only when velocities change with time. For a stationary, inflexible object situated in an accelerating fluid, the accelerational force is typically given by:

$$F_a = \rho Va + C_a\rho Va, \quad (5)$$

where C_a is the dimensionless added mass coefficient, V is the volume of fluid displaced by the object, a is the acceleration of the fluid relative to the object, and ρ is again the fluid's density. F_a acts in the direction of acceleration.

This force has two components. The first, ρVa, is the force that results from the pressure gradient associated with an accelerating fluid (Batchelor 1967). The second derives from a quantity of fluid that behaves as if it were part of the object; the so-called "added mass," $C_a\rho V$. This mass generates an additional force, $C_a\rho Va$ (Batchelor 1967, Denny 1988).

For an object with a constant added mass coefficient, the dual effects of the object plus its added mass are often combined into a single term, the inertia coefficient, C_m. This allows the accelerational force to be expressed simply as:

$$F_a = C_m\rho Va, \quad (6)$$

where C_m is $1 + C_a$ (see the Appendix for effects of a variable added mass coefficient).

Morison's equation

The total force parallel to flow (the in-line force) acting on a stationary object in unsteady flow is conventionally given by the sum of drag and the accelerational force:

$$F = F_d + F_a \quad (7)$$

$$= (1/2)C_d\rho A_c|u|u + C_m\rho Va, \quad (8)$$

an expression known as Morison's equation. Since the total force, F, depends on the precise nature and history of flow, as long as C_d and C_m are modeled as constants or simple functions, Eq. 8 can only approximate the actual force acting on an object. In general, Morison's equation is most accurate when applied to objects with nearly invariant C_d and C_m located in a fluid with constant, unidirectional acceleration (Sarpkaya and Tuter 1974, Sarpkaya and Isaacson 1981), an unlikely situation in real-world, time-dependent flows with vortex shedding and moving separation points. However, the Morison equation is the only expression available that has gained general acceptance for analyses in unsteady flow, and it has been used effectively in numerous laboratory studies, in particular several involving oscillatory motion. As such, the Morison equation is of considerable utility as long as its limitations as an approximate (rather than exact) representation of physical reality are not forgotten.

Harmonic flow

In harmonic oscillatory flow, velocity is sinusoidal:

$$u = u_{\max}\sin \phi, \quad (9)$$

where ϕ denotes the phase angle through a cycle, expressed in radians (SI symbol "rad"). $\phi = 2\pi t/T$ where t is time and T is the period of the oscillation. Acceleration (du/dt) therefore equals:

$$a = (2\pi/T)u_{\max}\cos \phi. \quad (10)$$

The drag force on an object is proportional to the square of velocity if C_d is constant (Eq. 1). Therefore, in harmonic flow, drag is zero at a phase angle of $\phi = 0$ and π, and is maximal at $\pi/2$ and $3\pi/2$ (Fig. 1). In contrast, for constant C_m, the accelerational force is proportional to a (Eq. 6), peaking at 0 and π and decreasing to zero at $\pi/2$ and $3\pi/2$. The net result is temporal separation of F_d and F_a: the accelerational force is zero at times of maximal drag, and is large when drag is zero (Fig. 1). Note that this temporal separation of drag and the accelerational force is a consequence of the sinusoidal velocity pattern characteristic of harmonic flow and need not occur for unsteady flow in general.

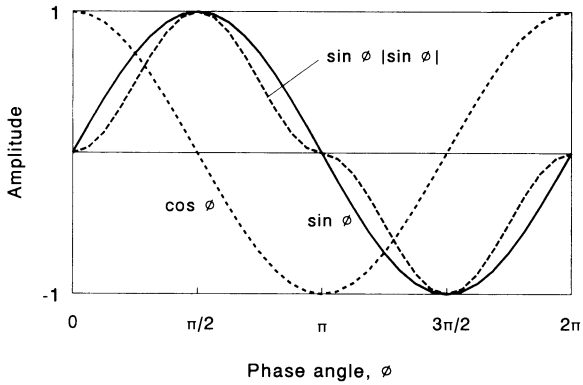

FIG. 1. In harmonic oscillatory flow, drag (F_d), which follows a sine|sine| function (essentially a modified sine wave), is out of phase with the accelerational force (F_a), which has a cosine character.

Splitting the force trace: Fourier analysis

Because the sinusoidal velocity pattern in harmonic flow produces drag and accelerational forces that are out of phase, it is possible to extract them separately from the total force. This is accomplished using Fourier analysis. In general, a periodic function $f(t)$ can be expressed as an infinite series consisting of the sum of sine and cosine terms (a Fourier series):

$$f(t) = \alpha_0/2 + \alpha_1\cos\phi + \alpha_2\cos 2\phi + \alpha_3\cos 3\phi + \ldots + \beta_1\sin\phi + \beta_2\sin 2\phi + \beta_3\sin 3\phi + \ldots, \quad (11)$$

where ϕ again symbolizes the phase angle ($2\pi t/T$) through a cycle. Since the total in-line force trace recorded in harmonic flow is periodic, it can be represented in the form of Eq. 11. The sine and cosine terms in this series can then be identified as drag or accelerational force components in the following manner. A sine|sine| function, which appears as a result of the $|u|u$ expression in Morison's equation (Eqs. 8 and 9), contains only odd sine harmonics when expanded in a Fourier series. Thus, for sinusoidal flow with constant C_d, the drag force in Morison's equation is represented purely by the summation of odd sine waves:

$$F_d = \sum_n \beta_n \sin n\phi, \quad n = 2i - 1, \quad i = 1, 2, 3, \ldots, \infty. \quad (12)$$

Conversely, because the accelerational force in harmonic flow with constant C_m varies cosinusoidally (Eqs. 8 and 10), the second term in Morison's equation (the accelerational force) can be approximated by a cosine term:

$$F_a = \alpha_1\cos\phi. \quad (13)$$

In this fashion, the drag and accelerational forces in harmonic flow can be distinguished from one another: the sum of the odd sine terms in the Fourier approximation of the force equals the drag and the cosine harmonic equals the accelerational force.

While in theory the nonlinearity of Morison's equation (due to the sine|sine| term) could corrupt results from the intrinsically linear Fourier approach, a sine|sine| function is mathematically "well-behaved" and can be accurately represented using the Fourier technique. Although the drag coefficients for the objects dealt with here typically decline with increasing velocity, and thus modify the sine|sine| function, this decrease in C_d essentially just offsets the nonlinearity of the drag function and does not compromise the method. We discuss this point in further detail below (see *Materials and methods: Data analysis: unsteady flow*).

MATERIALS AND METHODS

Species

Measurements were made primarily on three species of intertidal algae chosen to represent a broad range in morphology (Fig. 2). *Pelvetiopsis limitata,* a sturdy brown alga with a dichotomously branched thallus, and *Iridaea flaccida,* a red alga with a simple blade and a slightly curled or ruffled form, were collected at Garrapata State Beach south of Carmel, California. This site is fully exposed to oceanic waves, as evidenced by the presence of abundant stands of the sea palm, *Postelsia palmaeformis. Gigartina leptorhynchos,* a multibranched, bushy red alga, was collected at Hopkins Marine Station (HMS) in Pacific Grove, California. This site is subjected to smaller waves than those pres-

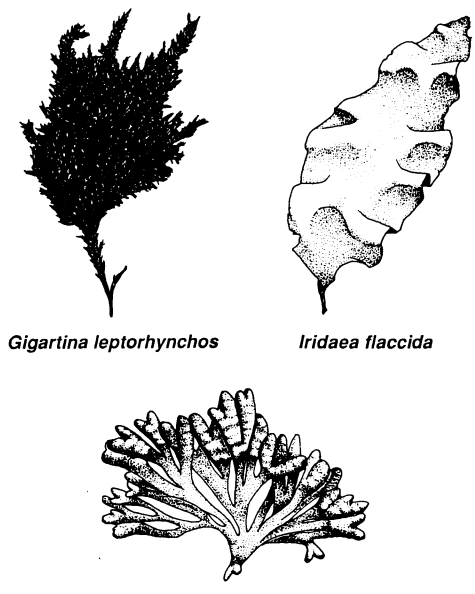

FIG. 2. The three primary species of algae used in this study.

ent at Garrapata Beach, having an exposure level we subjectively categorize as "moderately protected." Algae were identified according to Abbott and Hollenberg (1976) and maintained in running seawater at HMS for no longer than 2 d prior to use.

Measurements of algal strength

Breaking force was measured for 100 individuals each of *G. leptorhynchos* and *P. limitata* on three consecutive days in early September 1991 and for 100 individuals of *I. flaccida* on 1 d in June 1993. Several 10-m transects were randomly placed in the mid-intertidal zone where plants of the desired species were locally abundant, and individuals were haphazardly sampled along these transects until the goal of 100 plants was reached.

Breaking force for each of the 100 individuals from each species was determined using the method of Carrington (1990). One end of a short length of string was tied to a 5000-g spring scale (Ohaus, modified to record peak force), with the other end formed into a noose placed around the distal portion of the algal thallus. The spring scale was then pulled parallel to the substratum, simulating an in-line hydrodynamic force, until the thallus broke free. The force required to induce this mechanical failure was then recorded to the nearest 1 N. Although the algae typically failed at the narrowest part of the stipe, they occasionally broke in the vicinity of the string. Such breaking force values were considered potentially anomalous due to possible damage from the string and were discarded. Additionally, all samples that detached at the rock or rock/holdfast interface were not included in the analysis since these breaking force values likely reflected, at least in part, site-specific characteristics of the substratum itself, rather than species-specific organismal traits.

A, the maximal projected area of the plant (here used as the characteristic area, A_c, in Eqs. 1 and 8) was determined for each alga by pressing the plant between two plates of glass, photocopying it, and measuring the resulting area using an image processing program (SigmaScan, Jandel Scientific). During photocopying, a ruler was placed adjacent to the samples as a control to adjust the analysis for size distortion.

Algal volumes were estimated from their masses. The plants were shaken dry and blotted to remove excess surface water, then weighed to the nearest 0.01 g. The mass density of the algae was assumed to differ little from seawater; thus volumes (in cubic metres) were approximated by dividing masses (in kilograms) by 1025.

The within-species variation in algal strength (i.e., force to break) found during this sampling procedure was explored as follows. We first fit a curve to the model relationship between area and force:

$$\text{force} = z_1 + z_2 A^{z_3}. \tag{14}$$

The force to break each individual was then expressed as the ratio of its measured breaking force to the breaking force predicted by the regression of Eq. 14 for its species. The variation in this relative breaking force provides a means of estimating the probability that a plant chosen at random will have a strength exceeding a given value. The relative breaking forces for plants within a species were ranked in ascending order (the lowest relative force having rank 1) and the probability P of having a relative breaking force less than that of the plant with rank j was estimated as:

$$P = j/(N + 1), \tag{15}$$

where N is the total number of plants tested (in this case 100). A mathematical description of this cumulative probability distribution was then obtained using a modified Weibull model (see Table 3), fit to the probability data by a maximum likelihood, nonlinear, iterative estimate (SYSTAT, see Denny and Gaines [1990], Gaines and Denny [1993] for details on the fitting routine).

Measurements in steady flow

Drag was measured on individual plants in a recirculating unidirectional flow tank (Denny 1988). The thalli were either clamped or glued (using cyanoacrylate "super glue") at the base of the stipe to the planar platform of a force transducer (Denny 1989, Carrington 1990) placed flush with the wall of the flow tank. Drag acting on the alga was then recorded over a range of velocities from ≈ 0.5 to 3.0 m/s. The area, A, of each plant was measured as described above. Drag coefficients were calculated for each force measurement using a rearrangement of Eq. 1, where A is used as the characteristic area:

$$C_d \equiv 2F_d/(\rho A u^2). \tag{16}$$

Note that the inevitable variation in frontal area accompanying reconfiguration of a plant appears in this equation as a change in C_d.

The drag coefficient of a flexible object (defined as above) tends to decrease with an increase in velocity as the object bends and becomes more streamlined. An index of the decrease in C_d as a function of velocity can be found by fitting the measured data for drag as a function of velocity to the power curve:

$$F_d/A = z_4 u^{z_5}, \tag{17}$$

where z_4 and z_5 are coefficients determined by a simplex algorithm to give the least squares approximation to the untransformed data (Caceci and Cacheris 1984). For a bluff object at high Re, C_d is constant and $z_5 = 2$ (see Eq. 1). If C_d decreases with increasing velocity, $z_5 < 2$. The "Vogel number," $E = z_5 - 2$ (Vogel 1984), provides an alternative means of expressing the tendency for a drag coefficient to decrease with increasing velocity. E is zero for a bluff body and negative for objects that are either streamlined or reconfigure with increasing velocity to become more streamlined.

In addition to the three primary species already mentioned, drag measurements in steady flow were conducted on small individuals of *Calliarthron tuberculosum, Fucus distichus, Gigartina spinosa, Laurencia* sp., *Microcladia* sp., *Egregia menziesii,* and *Postelsia palmaeformis,* and on a variety of nonbiological shapes: a solid acrylic sphere of 2.17 cm diameter, a 4.1 cm diameter hollow plastic sphere with numerous 6 mm diameter holes (a "whiffle" golf ball), an identical perforated hollow sphere attached to a short (2.8 cm) string tether, a piece of plastic mesh shaped like an oblate ellipsoid (constructed from a portion of a "Tuffy" kitchen scrubber), and a flat sheet of flexible plastic (0.2 mm thick) cut to resemble an *I. flaccida* blade.

Measurements in unsteady flow

Individual plants and nonbiological objects were placed in an oscillating-flow tank, a 5.5 m high U-tube constructed from 30.5 cm diameter PVC (polyvinyl chloride plastic) pipe (Fig. 3). Its method of operation is as follows. The end of one arm is fitted with a set of computer-controlled solenoid valves, the first of which connects to a compressed air source and the other which opens to air at ambient pressure. The top of the second upright remains uncapped and the tank is filled with fresh water to a level halfway up the arms. By opening the valve to the compressed air and closing the other valve, a charge of high pressure air is periodically injected into the valved end of the tank. This pushes water downward in one arm and correspondingly upward in the opposite arm. When the valve to the compressed air closes and the other opens to outside air, gravity drives the displaced fluid back in the reverse direction. By administering the shot of compressed air at precise intervals, an oscillatory, near-sinusoidal velocity pattern is established in the tank. Converging tapers ("diffusers") speed the flow through the 100-cm^2 square cross section of the working section (Fig. 3), providing peak velocities and accelerations of ≈ 1 m/s and 0.8 m/s^2, respectively.

Test samples were mounted, one at a time, on a cantilever-style force transducer that converts force into a voltage signal (Denny 1988). This signal was monitored by an oscillographic chart recorder (Gould 220) simultaneously with the output from a Marsh-McBirney 523 miniature electromagnetic (EM) velocity meter (modified by Marsh-McBirney to have a response time of 0.05 s). To reduce noise due to turbulence, both inputs to the chart recorder were filtered using single pole RC filters with time constants of 1.5 s. Because both channels were identically filtered, no phase shift was introduced between channels (the 0.05-s internal filter in the EM probe prevents high-frequency aliasing but does not materially affect the phase relationship of the two channels). This was confirmed by applying a signal concurrently to both channels: they responded simultaneously. The base of each sample was attached to the force transducer via a mounting screw and held flush with the bottom of the tank. While the sensing element of the transducer was free to deflect in the direction of flow, the gap between the edge of the mounting screw and the rest of the tank bottom surrounding it was <3 mm. Thus any force resulting from interaction of flow with the mounting apparatus or transducer itself was minimal.

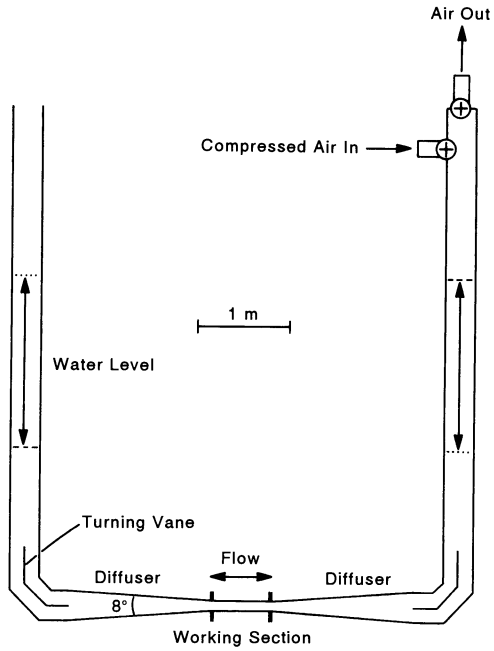

FIG. 3. U-tube apparatus used to produce harmonic oscillatory flow. Velocities and accelerations reach ≈ 1 m/s and 0.8 m/s^2, respectively, through the working section.

Due to space constraints, it was often necessary to locate the velocity probe near the wall of the working section, and under these conditions the probe gave artificially low readings. This artifact was not due to boundary layer effects but was electromagnetic in nature; such sensitivity to nearby surfaces is a well-known feature of the Marsh-McBirney EM probes. Velocity measurements made near the wall were therefore multiplied by an empirically determined correction factor to estimate flow in the center of the working section.

The velocity profile in the oscillating-flow tank is nearly uniform over any cross section through the working section. Not only do converging tapers lead into the working section to accelerate flow and retard boundary layer formation, but the boundary layer is further reduced by the velocity fluctuations (that is, accelerations) characteristic of oscillatory flow and by the periodic reversal of the direction of water motion, which acts to prevent the flow from becoming fully developed. The net result is a steep, turbulent boundary layer profile, for which conservative calculations (based on Schlichting 1979) indicate that velocities reach greater than 70% of mainstream within 3.5 mm from the wall. Visual estimates of bubble velocities in this region near the wall confirm these calculations.

Species tested in the oscillating-flow tank included *G. leptorhynchos, P. limitata,* and *I. flaccida.* Small (≈6 cm long), complete individuals were used when possible, rather than single or several thalli from larger plants. The larger size of *I. flaccida* necessitated using only single blades. Measurements in unsteady flow were also conducted on the solid sphere, perforated hollow sphere, tethered perforated hollow sphere, mesh ellipsoid, and the plastic sheet.

The period generated in the oscillating-flow tank was ≈8.0 s. With peak velocities on the order of 1.0 m/s and algal samples (as well as the plastic sheet) ≈6 cm in length, Reynolds numbers were on the order of 60 000 and period parameters ≈130. Corresponding values for the somewhat smaller solid sphere and mesh ellipsoid were 20 000 and 400, while the perforated spheres were tested at Re = 40 000 and K = 200. The period parameters in this study are thus in sharp contrast to those reported in a 1991 abstract of work by Koehl and coworkers (American Zoologist 31(4):60A), where K was ≈1 (M. A. R. Koehl, *personal communication*).

Note that in harmonic flow with u_{max} = 1 m/s and T = 8 s, only 0.5–0.6 s is required to reorient a flexible object 6 cm in length from its fully extended posture in one direction to that in the opposite direction. Thus, for the algae tested here, reorientation occupies only ≈12–15% of each half cycle of oscillation. During the remaining 85–88%, the object is fully extended in a fashion similar to that found in unidirectional flow.

Data analysis: unsteady flow

The use of Fourier analysis to separate drag and the accelerational force requires a sinusoidal velocity trace. However, velocities in the oscillating-flow tank were slightly asymmetrical as a result of being driven by the compressed air. To account for this, the forced half-cycles (i.e., those during which pressurized air was being injected) were discarded and modeled instead using the data from the unforced half-cycles transformed to operate in the opposite direction. This procedure yielded a velocity signal that closely resembled a pure sine wave.

Fourier coefficients for the total force trace were computed by numerical integration since the mathematical function representing the force trace was unknown and analytical integration was therefore impossible:

$$\alpha_n = (2/q) \sum_{k=0}^{q-1} [F_k \cos(n2\pi k/q)],$$

$$(n = 0, 1, 2, 3, \ldots, \infty) \quad (18)$$

and

$$\beta_n = (2/q) \sum_{k=0}^{q-1} [F_k \sin(n2\pi k/q)],$$

$$(n = 0, 1, 2, 3, \ldots, \infty). \quad (19)$$

In these equations, the term q corresponds to the number of points selected to define each cycle (32 in this experiment) and the ratio k/q is simply a discretized form of t/T. A Numonics digitizing pad was used to transfer values of the total in-line force and velocity at equally spaced time points (F_k and u_k) from the chart traces to a computer. At each k from 0 to 31, averages of F_k values from 10 cycles were then inserted into the equations above to obtain coefficients for the Fourier series approximation of the total in-line force. Since the sum of the first cosine and first three odd sine harmonics provided a curve nearly indistinguishable from actual measured data (all even coefficients, including the constant term α_0, were essentially zero) all higher harmonics were neglected.

The reconfiguration of algae typically results in C_d values that decrease with increasing velocity. This could cause concern since the method derived above for separating drag and the accelerational force implicitly assumes a constant drag coefficient. However, within quite general bounds, a C_d that declines exponentially does not qualitatively affect the Fourier spectrum; that is, although the relative magnitudes of β_1, β_3, and β_5 are altered, no new harmonics (neither even sine terms nor cosine terms) are introduced. Thus the Fourier method described above can be extended effectively to study forces on flexible algae in addition to rigid objects.

Once drag was extracted from the total force and the Fourier coefficients were determined, instantaneous C_d values through a cycle were estimated from:

$$C_d = [2/(\rho A |u| u)] \sum_n [\beta_n \sin n\phi],$$

$$(n = 1, 3, 5) \quad (20)$$

where the summation term above represents the Fourier approximation of the force due to drag (Eq. 12).

While in theory instantaneous values of the inertia coefficient could also be computed, the size of the accelerational force signal was small in our experiments, and as a result we have only limited confidence in the ability of our measurements to accurately resolve the fine-scale temporal variation of C_m through a cycle. We therefore made no attempt to describe any time-dependent behavior of the inertia coefficient, but instead computed a cycle-averaged value, $C_{m,avg}$. Consequences of this approximation are addressed in the *Discussion.*

Since acceleration was not measured directly, the slight nonsinusoidal characteristics of the unforced portion of the velocity trace were ignored and acceleration was modeled according to Eq. 10. In combination with Eqs. 6 and 13 this yields:

$$C_{m,avg} = F_a T/(2\pi\rho V u_{max} \cos\phi) \quad (21)$$

$$= \alpha_1 T/(2\pi\rho V u_{max}). \quad (22)$$

Similarly, cycle-averaged drag coefficients were computed as follows:

TABLE 2. Relative accelerational forces and force coefficients in unsteady flow.

Sample	Run	$F_{a,\max}/F_{\max}$ (percent)	$C_{m,\text{avg}}$	$C_{d,\text{avg}}$
Theoretical and empirical studies by others				
Solid sphere	...	...	1.5*	0.47†
	...	...	1.0‡	0.65‡
Present study				
Solid sphere	1	8.4	2.0	0.72
	2	9.4	2.6	0.67
Perforated hollow sphere	1	11.9	7.6 (2.0)§	0.88
	2	13.3	7.6 (2.0)§	0.87
Mesh ellipsoid	1	3.9	9.0 (3.0)§	1.45
	2	4.6	11.6 (3.9)§	1.46
Tethered perforated hollow sphere	1	5.7	3.3 (0.8)§	0.75
	2	3.6	1.9 (0.5)§	0.68
Plastic sheet	1	14.6	15.6	0.05
	2	16.4	19.2	0.05
G. leptorhynchos 1	1	4.0	4.6	0.46
	2	2.1	2.6	0.65
2	1	4.1	3.6	0.31
3	1	6.3	4.4	0.40
	2	8.8	6.1	0.34
P. limitata 1	1	10.7	6.2	0.42
	2	7.5	4.6	0.35
2	1	9.8	4.9	0.36
	2	11.3	6.3	0.47
3	1	8.9	6.2	0.39
I. flaccida 1	1	6.3	7.7	0.22
	2	7.0	6.3	0.22
	3	3.7	3.6	0.22
2	1	0.4	−0.5	0.25
	2	5.2	6.2	0.23
3	1	2.5	4.1	0.28

* Theoretical value for solid spheres in unidirectional flow with constant acceleration (Sarpkaya and Isaacson 1981).
† For spheres in nonaccelerating, unidirectional flow at $10^4 < \text{Re} < 10^6$ (Vogel 1981).
‡ For spheres far from a wall at Re 10^5, K 40 (Sarpkaya and Tuter 1974).
§ Parentheses indicate $C_{m,\text{avg}}$ values calculated as if these same objects were solid and had no internal cavities.

$$C_{d,\text{avg}} = [2/(\rho A q)] \sum_{k=0}^{q-1} [F_{d,k}/(|u_k|u_k)] \quad (23)$$

$$= [2/(\rho A q)] \sum_{k=0}^{q-1} \left\{ \left[\sum_n (\beta_n \sin(n2\pi k/q)) \right] \div (|u_k|u_k) \right\},$$

$$(n = 1, 3, 5) \quad (24)$$

where $F_{d,k}$ is the drag force at point k in a cycle.

The validity of the overall data analysis procedure was tested by measuring forces acting on spheres (a standard in the engineering literature) in our oscillating-flow tank, computing their average drag and inertia coefficients, and comparing the results to published data. The $C_{d,\text{avg}}$ values measured for a solid sphere in this study closely resembled those reported in other empirical studies using oscillatory flow (Table 2). Similarly, the $C_{m,\text{avg}}$'s found in the current test also matched available data quite well. Although our measurements yielded average inertia coefficients for spheres that were somewhat larger than those reported in other studies, this is to be expected because the present experiments were conducted with the spheres in close contact with the substratum. Sarpkaya (1976) reports that objects near a stationary, rigid surface can have inertia coefficients double those away from such surfaces. He also shows that, although the C_d's of objects can also be affected by their proximity to solid surfaces, this effect is much smaller than for C_m's.

Thus, although the current experiments were conducted at somewhat different flow conditions (indexed by Re and K), precluding exact comparisons to published results, the fit of our $C_{d,\text{avg}}$ and $C_{m,\text{avg}}$ values to other empirical data tentatively validates the experimental method and analysis technique used.

RESULTS

Breaking force

Breaking force was an increasing function of plant area for all three species of algae (*G. leptorhynchos, P.*

TABLE 3. Breaking force (in N) as a function of plant area (in m^2).

	Force = $z_1 + z_2 A^{z_3}$ (Eq. 14)				
	z_1	z_2	z_3	r^2	P
G. leptorhynchos	2.23	31.9	0.353	0.165	<0.001
P. limitata	8.66	260.7	0.494	0.167	<0.001
I. flaccida	0.00	44.8	0.260	0.087	<0.005
	Modified Weibull distribution for the probability, P, that a given relative breaking force is less than a value f': $P = \exp - \{[(\alpha - \beta f')/(\alpha - \beta\epsilon)]^{1/\beta}\}$				
	α	β	ϵ	r^2	P
G. leptorhynchos	0.376	0.129	0.881	0.985	<0.001
P. limitata	0.425	0.084	0.819	0.990	<0.001
I. flaccida	0.333	0.062	0.854	0.996	<0.001

limitata, and *I. flaccida*), although there was considerable variation around the regressions (Table 3). The estimated cumulative probability curves for the relative breaking force for all three algae are shown in Fig. 4, with the parameters of the Weibull model given in Table 3.

Steady flow

Drag coefficients vs. steady water velocity are shown for the three test species in Fig. 5, and for other objects in Fig. 6. For all the algae and the flexible plastic sheet, C_d decreased with increasing velocity. In other words, E values for the algae in steady flow were all below zero (Table 4), indicating that these plants were either streamlined or reconfigured to become more streamlined. The mean E for algae in our study was -0.40, with a range of -0.10 to -1.01.

For the bluff objects (solid sphere, perforated hollow sphere, mesh ellipsoid), C_d was virtually constant across velocities. That is, bluff objects all had E values very close to zero (Table 4).

Unsteady flow

Drag coefficients calculated from samples in oscillatory flow fell near those measured on the same specimens in steady flow (Figs. 5 and 6). For the three species of algae tested in oscillating flow, C_d values

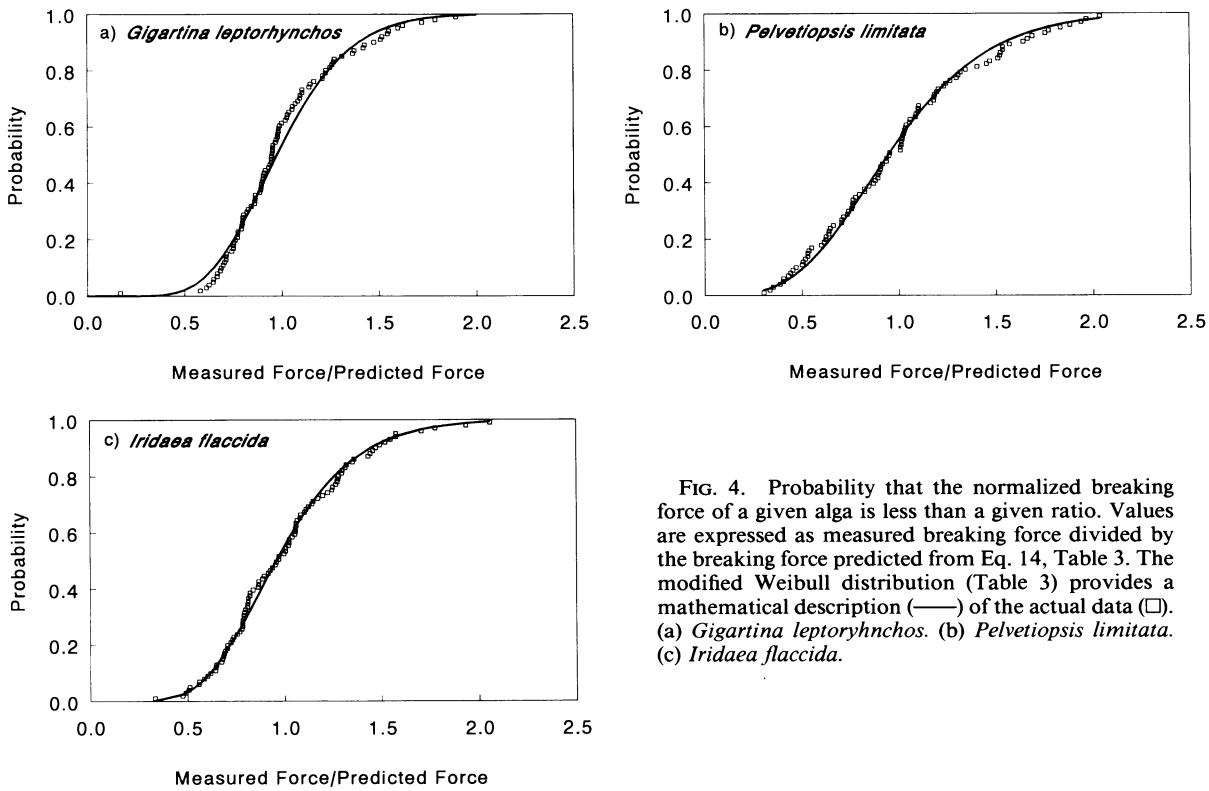

FIG. 4. Probability that the normalized breaking force of a given alga is less than a given ratio. Values are expressed as measured breaking force divided by the breaking force predicted from Eq. 14, Table 3. The modified Weibull distribution (Table 3) provides a mathematical description (——) of the actual data (□). (a) *Gigartina leptoryhnchos.* (b) *Pelvetiopsis limitata.* (c) *Iridaea flaccida.*

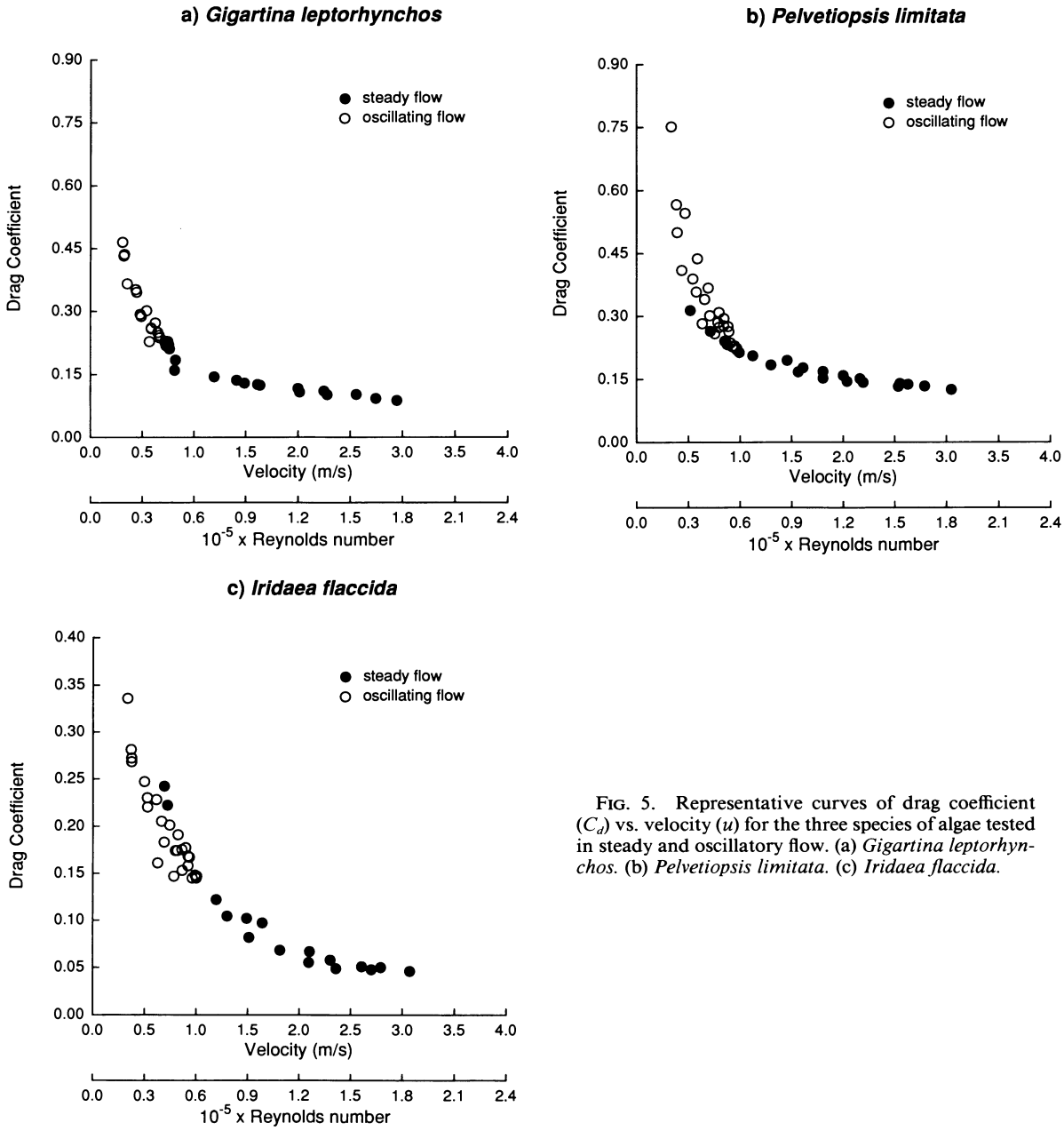

FIG. 5. Representative curves of drag coefficient (C_d) vs. velocity (u) for the three species of algae tested in steady and oscillatory flow. (a) *Gigartina leptorhynchos.* (b) *Pelvetiopsis limitata.* (c) *Iridaea flaccida.*

decreased with increasing velocity, with E ranging from -0.68 to -0.91.

Drag coefficients of the nonreorienting samples also showed a tendency, albeit a less striking one, to decline at higher velocities. This contrasted with C_d's found for the same nonreorienting objects in steady flow. Velocities in the oscillating-flow tank were limited to speeds between 0 and ≈ 1 m/s, however, so trends of C_d values in unsteady flow at higher velocities are unavailable.

Fourier analysis of the total in-line force records consistently yielded a force out of phase with velocity, indicating the presence of an accelerational force (Fig. 7). Fourier averaged values for C_m are given in Table 2. The solid sphere had a mean $C_{m,\text{avg}}$ of 2.3. Most other objects tested had substantially higher inertia coefficients. The hollow perforated spheres had $C_{m,\text{avg}}$ values of ≈ 7.6, and algae varied from 2.6 to 7.7 (the single exception, one trial for *I. flaccida,* will be addressed in the *Discussion: The reality of algal accelerational forces . . . : Limitations of the approach . . .*).

The large $C_{m,\text{avg}}$'s of the perforated hollow spheres and mesh ellipsoid provide clues as to why algae also possess large inertia coefficients. When $C_{m,\text{avg}}$ calculations for the perforated spheres and the mesh ellipsoid were performed using volume terms as if these objects

TABLE 4. Vogel number, E, of various species and nonbiological shapes at moderate to high Reynolds numbers.

Object	Condition*	E		Source
		Steady flow	Oscillating flow	
		Nonbiological		
Bluff body (sphere, cylinder, cube, disk, or flat plate broadside to flow)	Re > 10^6	0.00	···	Fox and McDonald 1985†
Sphere	Re 3000–10^5	+0.13	···	Massey 1989†
	Re 16 000–7 × 10^4	+0.05	···	Present study
	Re 20 000, K 400	···	−0.31	Present study
Perforated hollow sphere	Re 20 000–1.5 × 10^5	−0.02	···	Present study
	Re 40 000, K 200	···	−0.22	Present study
Tethered perforated hollow sphere	Re 20 000–1.5 × 10^5	−0.06	···	Present study
	Re 40 000, K 200	···	−0.10	Present study
Circular cylinder, normal to flow	Re 3000–10^5	+0.09	···	Massey 1989†
Mesh ellipsoid	Re 10^4–7 × 10^4	0.00	···	Present study
	Re 20 000, K 200	···	−0.23	Present study
Streamlined body				
Smooth	Re 10^7–10^8	−0.20	···	Hoerner 1965†
	Re 10^3–10^5	−0.50	···	Hoerner 1965†
Rough	Varies with roughness; (typical of Re > 10^6)	0.00	···	Hoerner 1965†
	(typical of Re 1000–10^4)	−0.20	···	Hoerner 1965†
Flat plate parallel to flow	Re 10^7–10^9	−0.16	···	Schlichting 1979†
	Re 5 × 10^5–10^7	−0.20	···	Schlichting 1979†
	Re 3 × 10^4–3 × 10^5	−0.44	···	M.W. Denny, *unpublished data*
	Re 10^3–5 × 10^5	−0.50	···	Schlichting 1979†
Rough flat plate parallel to flow	Varies with roughness; (typical of Re > 10^6)	0.00	···	Hoerner 1965†
	(typical of Re 1000–10^4)	−0.20	···	Hoerner 1965†
Plastic sheet	Re 30 000–2 × 10^5	−1.05	···	Present study
	Re 5 × 10^4–10^5	−0.55	···	Vogel 1989
	Re 60 000, K 130	···	−0.90	Present study
		Trees		
Acer rubrum, leaf	10–20 m/s air	−0.79	···	Vogel 1989
Acer rubrum, leaf cluster	10–20 m/s air	−0.64	···	Vogel 1989
Carya glabra, leaflet	10–20 m/s air	−0.20	···	Vogel 1989
Carya glabra, leaf	10–20 m/s air	−0.78	···	Vogel 1989
Ilex opaca	8–19 m/s air	−1.30	···	Vogel 1984
Ilex opaca, branch	8–19 m/s air	−0.10	···	Vogel 1984
Juglans nigra, leaf	10–20 m/s air	−0.76	···	Vogel 1989
Liriodendron tulipifera, leaf	10–20 m/s air	−1.18	···	Vogel 1989
Liriodendron tulipifera, leaf cluster	10–20 m/s air	−0.91	···	Vogel 1989
Pinus sylvestris	9–38 m/s air	−0.72	···	Vogel 1984
Pinus taeda	8–19 m/s air	−1.13	···	Vogel 1984
Pinus taeda, branch	8–19 m/s air	−1.16	···	Vogel 1984
Populus alba, leaf cluster	10–20 m/s air	−0.60	···	Vogel 1989
Quercus alba, leaf	10–20 m/s air	+0.97	···	Vogel 1989
Quercus alba, leaf cluster	10–20 m/s air	−0.44	···	Vogel 1989
Quercus phellos, leaf cluster	10–20 m/s air	−1.06	···	Vogel 1989
Robinia pseudoacacia, leaf	10–20 m/s air	−0.52	···	Vogel 1989
		Freshwater algae		
Audouinella violacea	0.2–0.75 m/s	−0.92	···	Sheath and Hambrook 1988
Batrachospermum boryanum	0.2–0.75 m/s	−0.33	···	Sheath and Hambrook 1988
Batrachospermum moniliforme	0.2–0.75 m/s	−0.65	···	Sheath and Hambrook 1988

TABLE 4. Continued.

Object	Condition*	E: Steady flow	E: Oscillating flow	Source
Batrachospermum virgatum	0.2–0.75 m/s	−0.45	···	Sheath and Hambrook 1988
Lemanea fucina	0.2–0.75 m/s	−0.83	···	Sheath and Hambrook 1988
Sirodotia suecica	0.2–0.75 m/s	−1.27	···	Sheath and Hambrook 1988
Tuomeya americana	0.2–0.75 m/s	−0.64	···	Sheath and Hambrook 1988
	Marine macroalgae			
Calliarthron tuberculosum	0.5–3 m/s	−0.34	···	Present study
Egregia menziesii	0.5–3 m/s	−0.49	···	Present study
Eisenia arborea	0.2–0.6 m/s	−0.68	···	Charters et al. 1969†
Endocladia muricata	0.5–4 m/s	−0.48	···	Carrington 1990
Fucus distichus	0.5–4 m/s	−0.50	···	Carrington 1990
	0.5–3 m/s	−0.32	···	Present study
Gigartina exasperata				
Near substratum	0.1–0.5 m/s	−0.48	···	Koehl 1984†
Far from substratum	0.1–0.5 m/s	−0.25	···	Koehl 1984†
Gigartina leptorhynchos	0.5–4 m/s	−0.52	···	Carrington 1990
	0.5–3 m/s	−0.55	···	Present study
	1 m/s, *K* 130	···	−0.68	Present study
Gigartina spinosa	0.5–3 m/s	−0.10	···	Present study
Hedophyllum sessile	0.5–2.5 m/s	−1.20	···	Armstrong 1984
Iridaea flaccida	0.5–4 m/s	−0.76	···	Carrington 1990
	0.5–3 m/s	−1.01	···	Present study
	1 m/s, *K* 130	···	−0.91	Present study
Laurencia sp.	0.5–3 m/s	−0.27	···	Present study
Mastocarpus jardinii	0.5–4 m/s	−0.28	···	Carrington 1990
Mastocarpus papillatus	0.5–4 m/s	−0.38	···	Carrington 1990
Microcladia sp.	0.5–3 m/s	−0.16	···	Present study
Nereocystis luetkeana				
Undulate and wide	1.3–2.0 m/s	−0.73	···	Koehl and Alberte 1988†
Flat and narrow	1.3–2.0 m/s	−1.11	···	Koehl and Alberte 1988†
Pelvetia fastigiata	0.5–4 m/s	−0.33	···	Carrington 1990
Pelvetiopsis limitata	0.5–3 m/s	−0.48	···	Present study
	1 m/s, *K* 130	···	−0.83	Present study
Postelsia palmaeformis	0.5–3 m/s	−0.30	···	Present study
Sargassum filipendula	0.2–1.5 m/s	−1.06	···	Vogel 1984
	Flexible invertebrates			
Ptilosarcus gurneyi	0.02–0.26 m/s	−0.86	···	Vogel 1984
	0.11–0.26 m/s	−1.14	···	Vogel 1984

* Velocities and Reynolds number reported for oscillating flow refer to peak values in a cycle, whereas the Re and velocities given for steady flow refer to ranges.

† Vogel number, *E*, was not explicitly reported in this source, but was calculated from data shown in tables or graphs.

were solid, their inertia coefficients dropped by a factor of 3 or 4. For the stationary perforated hollow sphere, this yielded $C_{m,\text{avg}}$ values quite near those obtained for the solid sphere. Algal inertia coefficients fell midway between those of the objects with large enclosed volumes (i.e., the perforated hollow sphere and mesh ellipsoid) and those of the solid sphere. These results suggest that the high $C_{m,\text{avg}}$ values for algae are at least in part due to the tendency for these organisms to trap within the interstices of their thalli a volume of water that is inhibited from flowing with the mainstream. Just as the perforated hollow sphere traps within itself a volume of water and thereby experiences an accelerational force similar to that of a solid sphere of equal diameter, an alga enclosing fluid may also develop a large accelerational force.

DISCUSSION

Drag coefficients in steady and oscillatory flow

Our measurements reconfirm those of Vogel (1984, 1989), Sheath and Hambrook (1988), and Carrington (1990) showing that the drag coefficients of flexible plants decrease with increasing velocity. Our measurements were limited to maximal velocities of 3 m/s by the capabilities of our flow tanks, but a linear decrease in the logarithm of C_d with an increase in the logarithm of velocity is evident in our data (Fig. 8), allowing for a tentative extrapolation to higher velocities (Fig. 9, Table 5). These extrapolations suggest that at velocities high enough to load plants near their breaking strength

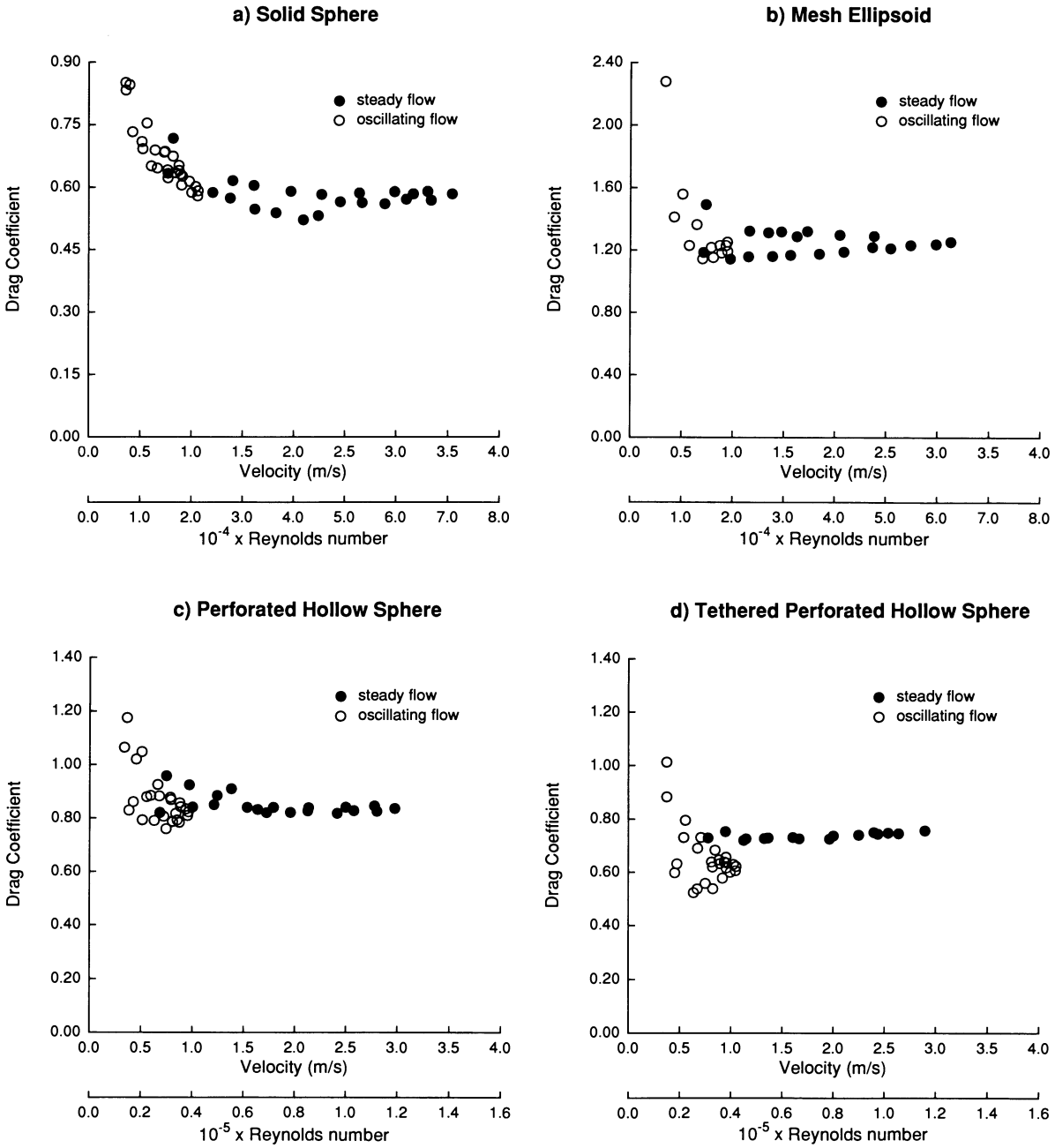

FIG. 6. Representative curves of drag coefficient (C_d) vs. velocity (u) for the nonbiological objects tested in steady and oscillatory flow. (a) Solid sphere. (b) Mesh ellipsoid. (c) Perforated hollow sphere. (d) Tethered perforated hollow sphere. (e) Plastic sheet.

(>10 m/s) flexible intertidal macroalgae, regardless of their still-water morphology, have drag coefficients (based on maximal projected area) typical of moderately streamlined objects (<0.1, Hoerner 1965). As discussed above, this presumably results largely from plant reconfiguration to a more streamlined posture as velocities increase.

Our results, however, also suggest that oscillatory flow may produce a decrease in C_d with increasing water velocity even when reconfiguration does not occur. For example, the drag coefficient of the solid sphere in oscillating flow dropped by ≈30% over the velocity range 0.5–1.0 m/s, as did the drag coefficient for the mesh ellipsoid (Fig. 6). Analogously, the E values calculated for drag on flexible objects in oscillatory flow are, in general, slightly lower than those in unidirectional steady flow (Table 4). Thus, it is possible that characteristics of oscillatory flow intrinsically lead to

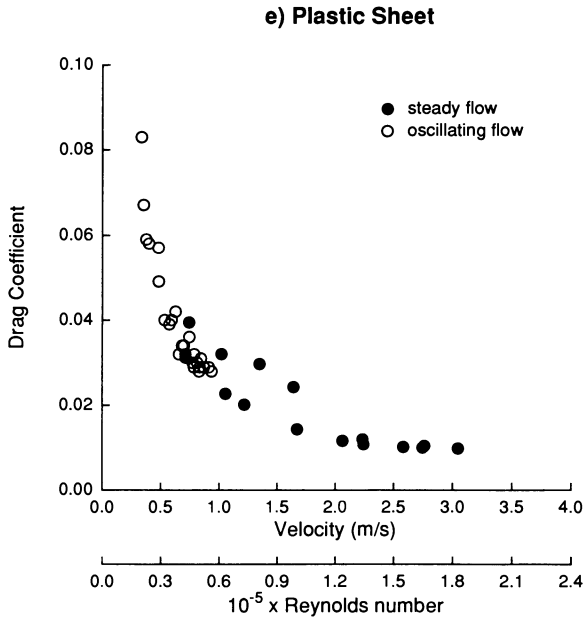

FIG. 6. Continued.

C_d's that fall with increasing velocity and may enhance the rate at which drag coefficients of reconfiguring organisms decline. The present data, however, are merely suggestive; further testing will be required to determine if a secondary mechanism for generating negative E values (i.e., other than reconfiguration) indeed exists.

Size limitation by drag alone

Is the force imposed on intertidal algae by drag alone sufficient to limit their size? We explored this question in the following manner. Denny (1991, 1993), based on empirical data from Denny and Gaines (1990), suggests that the predicted maximal drag force imposed on a wave-swept organism is:

$$F_{d,\max} = (1/4)M_{y,\max}{}^2 H_m{}^2 \rho C_d A, \qquad (25)$$

where $M_{y,\max}$ is the ratio of the predicted maximal wave height to the mean significant wave height, H_m, a measure of the average "waviness" of the ocean at a particular site (Denny 1988, 1991). $M_{y,\max}$ is a function of time and of the distribution of significant wave heights. Data presented by Denny (1991, 1993) suggest that the shape of the distribution of significant wave heights is similar among sites on the west coast of North America, allowing one to calculate approximate values of $M_{y,\max}$ for different time spans. $M_{y,\max}$ for a period of 3 mo is $\approx$5.5, and for 12 mo is $\approx$6.4. In other words, in a period of 3 mo, the highest wave impinging on a site is likely to be $\approx$5.5 times the mean significant wave height at that site for that period. In a year the highest wave is likely to be 6.4 times H_m.

Note that Eq. 25 is based on the assumption that the flow relative to an organism is equal to the mainstream flow. As a result, it cannot be expected to apply to organisms that move with the flow for a substantial portion of each wave period. This limitation does not pose a problem for tests of the algal species dealt with in this study (where $K > 100$ and reorientation occurs over only a short fraction of an oscillatory cycle), but may be problematic in any attempt to extend the results obtained here to flexible intertidal algae that are exceptionally long (e.g., *Egregia menziesii*).

The drag coefficient used in Eq. 25 is that which operates at the velocity imparted by the wave causing the maximal force. A theoretical estimation of this velocity requires the application of wave theories that are of unproven accuracy in the surf zone of rocky shores. As a practical alternative, we assume that the maximal velocity is $\approx$15 m/s, near the maximal value obtained from field measurements. The $C_{d,\text{avg}}$ values listed in Table 2 apply only at low velocities and are inappropriate for computing drag at faster flow speeds. Instead, we extrapolate from the data of Fig. 5 to estimate C_d's at higher velocities (Table 5). Note that for

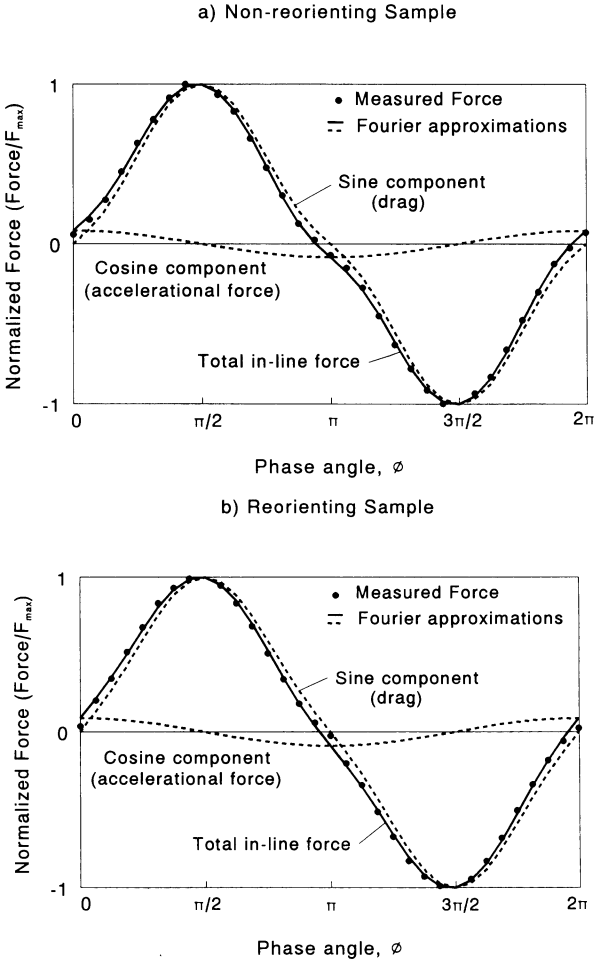

FIG. 7. Representative examples showing the forces on (a) nonreorienting and (b) reorienting samples in oscillating flow. The accelerational component is typically $\approx$10% as large as the drag force.

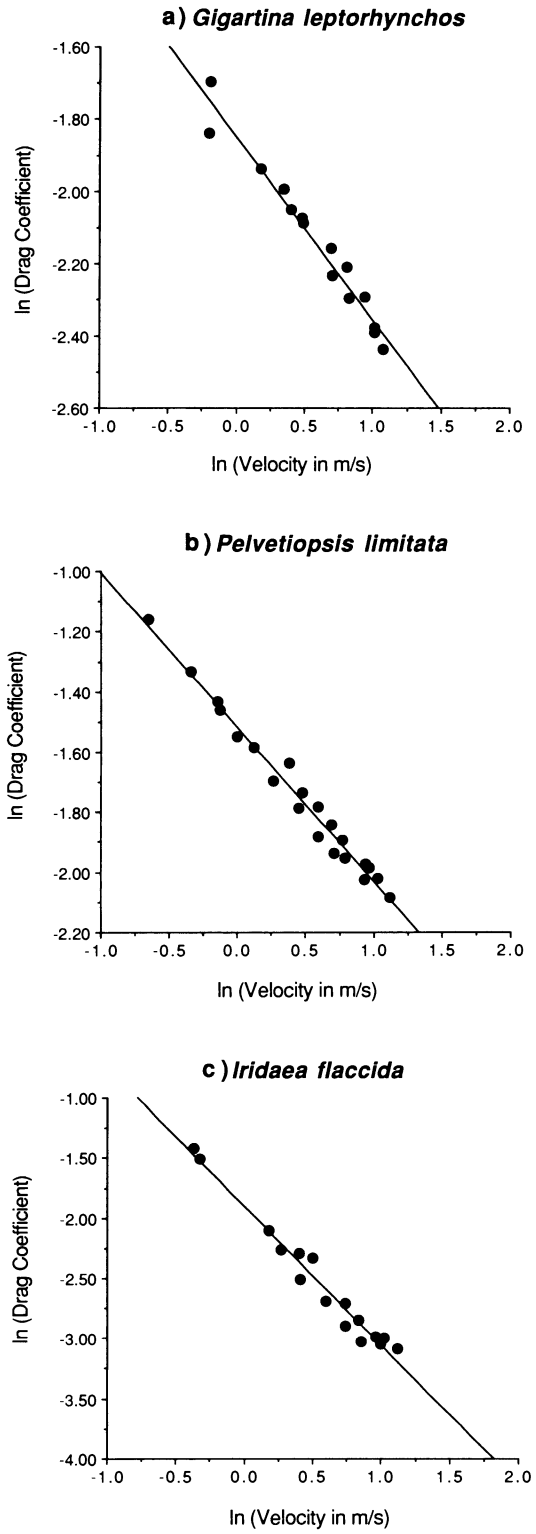

FIG. 8. Representative log transforms of the steady-flow data shown in Fig. 5, demonstrating the linear relationship between $\ln(C_d)$ and $\ln(u)$. (a) *Gigartina leptorhynchos*. (b) *Pelvetiopsis limitata*. (c) *Iridaea flaccida*.

the algae used in this study, these estimates of C_d do not vary substantially over the range of water velocities 10–20 m/s (Fig. 9), so the use of a single drag coefficient calculated for $u = 15$ m/s applies equally well to a wide range of maximal velocities.

We use the relationship of Eq. 25 to estimate the maximal drag imposed on algae of different thallus area in periods of 3 and 12 mo for mean significant wave heights of 1 m (a typical yearly value for a moderately protected site) and 2 m (a typical yearly value for an

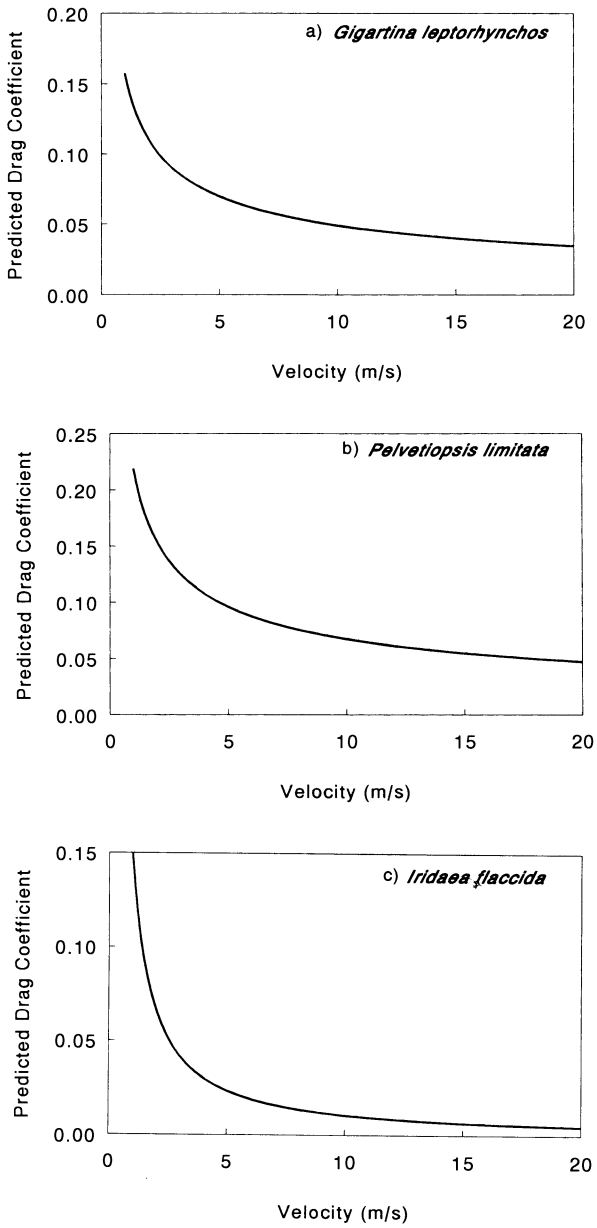

FIG. 9. Representative extrapolations, using the linear relationships of Fig. 8 and Table 5, to large velocities. Note that the drag coefficient, C_d, is essentially constant at higher flow speeds. (a) *Gigartina leptorhynchos*. (b) *Pelvetiopsis limitata*. (c) *Iridaea flaccida*.

TABLE 5. Extrapolation of C_d's to velocities of 15 m/s in steady flow.

Alga	Sample	C_d	Regression
G. leptorhynchos	1	0.094	$\ln(C_d) = -1.187 - 0.436 \ln(u)$, $r^2 = 0.809$, $P < 0.001$
	2	0.040	$\ln(C_d) = -1.848 - 0.507 \ln(u)$, $r^2 = 0.964$, $P < 0.001$
	3	0.046	$\ln(C_d) = -1.602 - 0.545 \ln(u)$, $r^2 = 0.846$, $P < 0.001$
		Mean 0.060	
P. limitata	1	0.047	$\ln(C_d) = -1.688 - 0.504 \ln(u)$, $r^2 = 0.966$, $P < 0.001$
	2	0.055	$\ln(C_d) = -1.518 - 0.512 \ln(u)$, $r^2 = 0.980$, $P < 0.001$
	3	0.092	$\ln(C_d) = -1.279 - 0.409 \ln(u)$, $r^2 = 0.973$, $P < 0.001$
		Mean 0.065	
I. flaccida	1	0.008	$\ln(C_d) = -2.431 - 0.876 \ln(u)$, $r^2 = 0.927$, $P < 0.001$
	2	0.007	$\ln(C_d) = -1.900 - 1.154 \ln(u)$, $r^2 = 0.972$, $P < 0.001$
	3	0.005	$\ln(C_d) = -2.159 - 1.141 \ln(u)$, $r^2 = 0.921$, $P < 0.001$
		Mean 0.007	

exposed site). Each value of predicted maximal force was then used in conjunction with the strength distribution data for a species (Fig. 4) to estimate the probability that a plant of that size would survive the given period. These data are shown in Fig. 10.

Although large size imposes an increased risk of breakage, the risk from drag alone is in general low for the three species tested here. Only if *G. leptorhynchos* of the size present at our moderately protected collection site (mean $A = 0.0039$ m^2, estimated $H_m = 1$ m) were in fact present at an exposed site (estimated $H_m = 2$ m) and maintained the same strength distribution, would an individual's probability of survivorship be materially reduced. Under these conditions, a *G. leptorhynchos* plant would have a probability of $\approx 40\%$ of surviving for 3 mo, and $< 10\%$ of surviving for an entire year. Note, however, that we never observed this species at our exposed collection site.

For the other test species, drag alone has essentially no impact on the predicted survivorship of plants in the observed size range. For example, the probability of surviving drag for a year on an exposed shore is $>90\%$ for a typical *P. limitata* individual (mean $A = 0.0034$ m^2, Fig. 10). This high probability of survival is primarily due to the relatively high strength of this alga. The yearly probability of survival of a typical *I. flaccida* individual (mean $A = 0.0083$ m^2) would be $>99\%$ on an exposed shore. In this case, the high probability of survival is due primarily to *I. flaccida* having a lower drag coefficient than *G. leptorhynchos*.

At more protected sites ($H_m = 1$ m), the probability of surviving drag forces alone remains high to sizes many times those actually observed for all species examined here.

These results raise the question of whether drag by itself typically constrains the size of intertidal algae. We explore this question further by calculating an index of reproductive output for our test species.

The number of gametes or spores an alga can produce can be modeled as being proportional to the individual's volume. If we ignore perennation and vegetative propagation due to fragmentation, an index of the realized reproductive output of an individual is therefore the product of plant volume and the probability that the individual will survive intact to the time of reproduction, a function of plant area as shown in Fig. 10. We emphasize that although this theoretical linkage of volume to reproductive capacity is likely to be sufficiently realistic for the first-order model used in this study, we have no data that directly substantiate this simplification.

Volume can then be expressed as an allometric function of A:

$$V = z_6 A^{z_7}, \tag{26}$$

where z_6 and z_7 are coefficients determined by a least squares fit to the volume–area data, calculated using a simplex algorithm applied to the untransformed data. This allows the index of reproductive output to be represented as a function solely of plant area (which we use as an index of size). Values for z_6 and z_7 are given in Table 6 for the species examined here. Note that for *I. flaccida*, z_7 is almost exactly 1, indicative of the fact that this species grows as a thin sheet.

The results of this analysis are shown in Fig. 11. Predicted reproductive output increases with an increase in plant area, but only up to a certain size. Above this size, the low probability of survival due to drag begins to offset the increase in the number of gametes or spores produced, and reproductive output declines. Thus, for these intertidal algae the effects of drag in conjunction with the plants' morphology determine a rough size at which their reproductive output is maximal. The more wavy the ocean (i.e., the higher the H_m) and the longer the period of growth leading up to reproduction, the smaller the predicted optimal size.

The predicted optimal size, A_{opt}, for *G. leptorhynchos* subjected to drag alone at an exposed site ($H_m = 2$ m) is near the mean size we observed in this species ($A_{opt} = 0.0020$ m^2 for 12 mo survival, 0.0029 m^2 for 3 mo, mean $A = 0.0039$ m^2, Fig. 11). We again note, however, that these plants were collected not at an exposed site, but at a more protected location where H_m is only ≈ 1 m. In contrast, the predicted optimal size of *G. leptorhynchos* with $H_m = 1$ m is 3–5 times the size actually observed ($A_{opt} = 0.0128$ m^2, 0.0196 m^2 for a 12- or

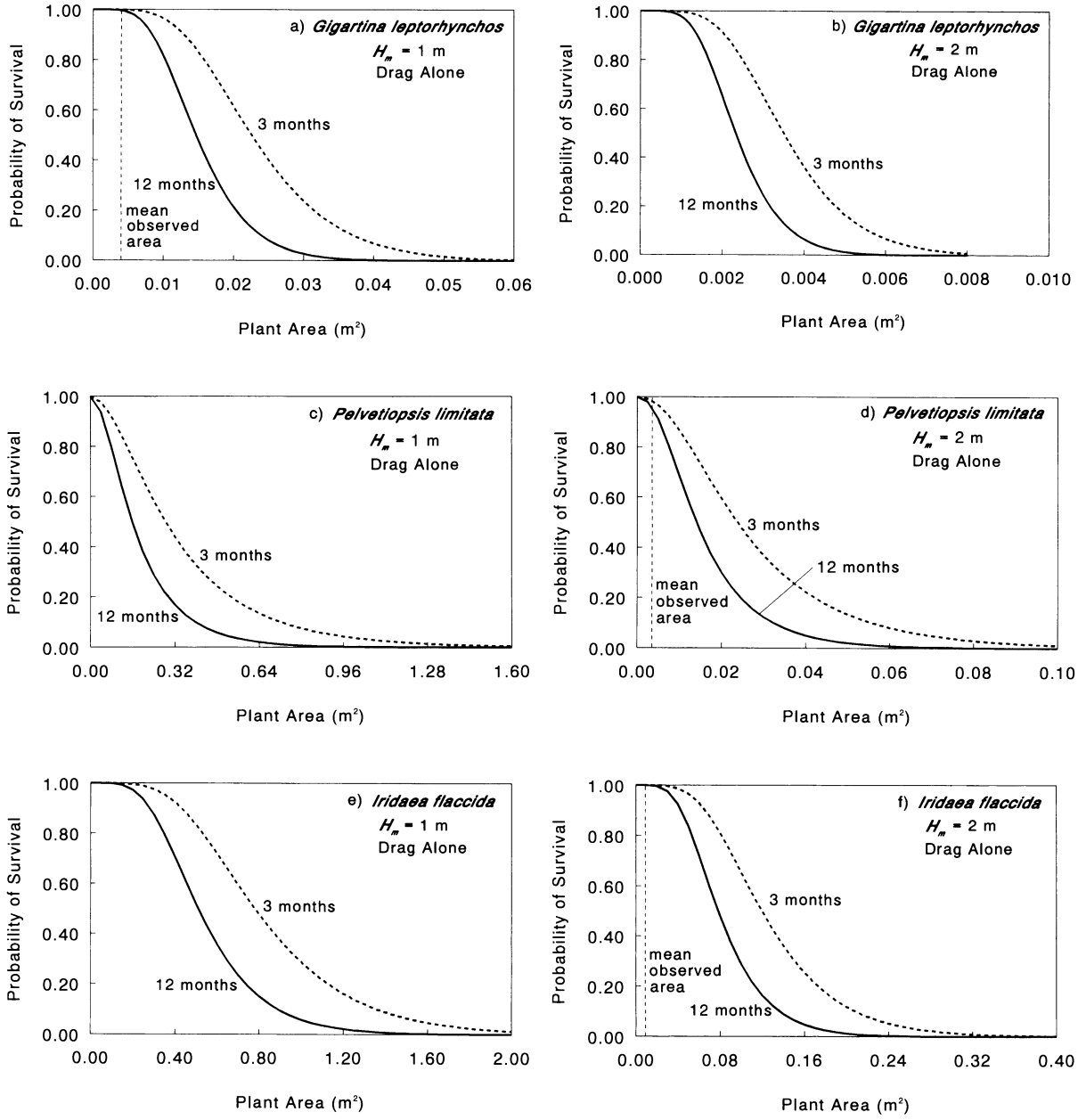

FIG. 10. Predicted survivorship at 3 and 12 mo vs. plant area, for three species of algae. The mean observed areas for each species are shown in panels where H_m matches that of the site where the plants were collected. In this graph, only forces from drag alone are considered. (a) *Gigartina leptorhynchos* at a moderately protected site (H_m = 1 m). (b) *Gigartina leptorhynchos* at an exposed site (H_m = 2 m). (c) *Pelvetiopsis limitata*, H_m = 1 m. (d) *Pelvetiopsis limitata*, H_m = 2 m. (e) *Iridaea flaccida*, H_m = 1 m. (f) *Iridaea flaccida*, H_m = 2 m.

3-mo period, respectively). Similarly, the predicted optimal size of *P. limitata* on an exposed shore (such as where we collected this species) is 5–9 times the size observed (A_{opt} = 0.0170 m², 0.0290 m², mean A = 0.0034 m²), and at a site characterized by H_m = 1 m it is 60–100 times that actually observed (A_{opt} = 0.2070 m², 0.3850 m²). The predicted optimal size for *I. flaccida* at an exposed site is 7–11 times that actually observed at our exposed collection site (A_{opt} = 0.0595 m², 0.0915 m², mean A = 0.0083 m²), and at a protected site the predicted optimum is 40–70 times this size (A_{opt} = 0.3882 m², 0.5953 m²).

The implications of these data are twofold. First, the above analysis confirms a portion of the argument proposed by Carrington (1990). During growth, the size of thalli of the algae examined here (like those of *Mas-*

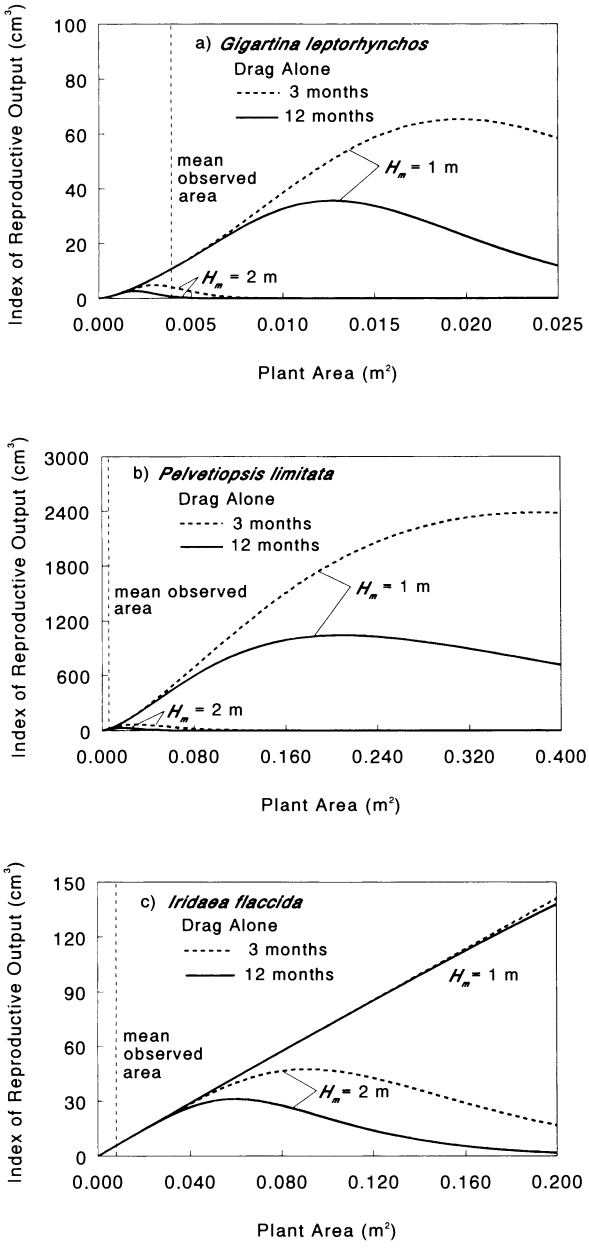

FIG. 11. Index of reproductive output for a 3- and 12-mo period vs. plant area, for three species of algae growing either at a moderately protected site (H_m = 1 m) or at an exposed site (H_m = 2 m). Here, only forces from drag alone are considered. (a) Predicted optimal plant areas for *Gigartina leptorhynchos* at an exposed location are near the mean size observed; predicted optimal sizes for a moderately protected site are not. Note that this species was collected at a moderately protected location. Observed mean sizes for (b) *Pelvetiopsis limitata* and (c) *Iridaea flaccida* are much smaller than the predicted optima at both protected and exposed sites.

tocarpus papillatus) increases out of proportion to their strength. As a result, an alga is limited to some effective maximal size set by its drag coefficient and the largest water velocity it is likely to encounter. However, based on the risks of drag alone, we would predict that at H_m's matching the exposure at each species' respective sampling site, *G. leptorhynchos, P. limitata,* and *I. flaccida* could (and in terms of their reproductive output, should) grow to be many times the sizes observed. Thus we may also draw a second conclusion: drag alone apparently is not a primary factor constraining the size of these species of algae.

TABLE 6. Constants in the allometric function, $V = z_6 A^{z_7}$ (Eq. 26).

Alga	z_6	z_7	r^2	P
G. leptorhynchos	6.24×10^{-3}	1.24	0.750	<0.001
P. limitata	27.08×10^{-3}	1.41	0.947	<0.001
I. flaccida	1.45×10^{-3}	0.99	0.852	<0.001

We therefore turn our attention to the magnitude of accelerational forces of algae and to the possibility that these forces may set a more restrictive constraint on the size of these plants.

Biological consequences of the accelerational force

Large algal inertia coefficients.—Many algae are highly branched, have intricate foliose structure, and may have numerous small interstices that can hold water. Thus, like the perforated hollow spheres and mesh ellipsoid, these organisms have the potential for trapping significant amounts of fluid and might therefore be expected to possess large inertia coefficients. Indeed, tests on *Gigartina leptorhynchos* and *Pelvetiopsis limitata* showed sizable $C_{m,\mathrm{avg}}$'s. However, large $C_{m,\mathrm{avg}}$ values were also found for *Iridaea flaccida,* a species that superficially does not appear capable of trapping much fluid at all, as well as for the plastic sheet (Table 2).

At first glance, the large inertia coefficient for *I. flaccida* appears perplexing. But *I. flaccida,* although sheet-like, often curls in flow, enclosing fluid much as the tortilla of a burrito encloses beans (Fig. 12). This behavior was also observed with the strip of plastic. The ratio of enclosed fluid volume to plant volume may in fact be higher for sheet-like plants than for more bushy plants such as *G. leptorhynchos.*

FIG. 12. Schematic representation of an *Iridaea flaccida* blade in flow. By curling up, a blade may enclose fluid and develop a large inertia coefficient, despite its sheet-like form.

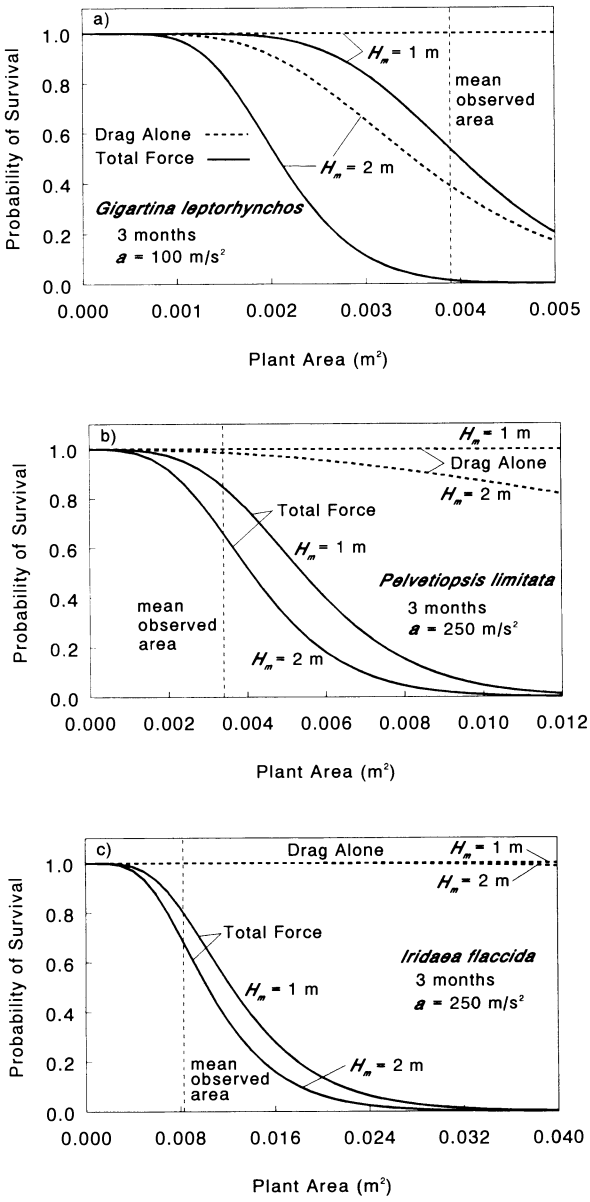

FIG. 13. Probability of surviving 3 mo for three species of algae growing at two different exposures (H_m = 1 m, 2 m). Here, the addition of the accelerational force to drag (yielding the total in-line force) greatly reduces survivorship at larger plant sizes. The total-force survivorship curves for 1 yr are nearly identical to those for 3 mo, so only data for 3 mo are shown. Calculations were made using accelerations appropriate for the level of exposure typical of the sites where each species was collected. (a) *Gigartina leptorhynchos* subjected to accelerations of 100 m/s², realistic for a moderately protected site. (b) *Pelvetiopsis limitata* subjected to accelerations of 250 m/s², realistic for an exposed site. (c) *Iridaea flaccida* subjected to accelerations of 250 m/s².

The fact that intertidal algae are sessile may also contribute to their sizable inertia coefficients. The C_m's of objects can increase substantially with close proximity to the substratum. Sarpkaya (1976) reports $C_{m,\mathrm{avg}}$ values for cylinders within a cylinder radius of the bottom that are more than twice as large as the inertia coefficients of cylinders far from a rigid surface. Thus algae, as a consequence of being attached to the substratum, have at least part of their length confined to a region where C_m's are potentially elevated. This leads to an interesting conjecture. By bending over with flow, algae become more streamlined, lowering their C_d's and the drag forces they experience. Yet in the process of "going with the flow," these plants also assume a position where near-wall effects may enlarge their inertia coefficients. Thus, even as the flexible nature of algae allows them partially to elude forces from steady flow, this same compliance may make them more vulnerable to accelerating flow. Whether this phenomenon actually occurs with algae, however, has not yet been tested.

The accelerational force as an operational constraint on size.—Given the capacity of intertidal macroalgae to develop large inertia coefficients, these organisms can be expected to experience sizable accelerational forces despite their relatively small size. We now focus on the effects of these forces.

At present there is no method by which we can estimate the acceleration that accompanies a given velocity in a breaking wave. As a practical alternative, we follow the approach of Denny et al. (1985) and specify a reasonable acceleration based on available measurements. Denny et al. (1985) recorded accelerations in the surf zone in excess of 400 m/s² and suggest that accelerations as high as 1000–2000 m/s² may occur in winter storms. These are accelerations relative to rigid objects firmly attached to the rock substratum. Flexible objects such as the algae used in this study are likely to experience somewhat lower effective accelerations (Koehl 1984), and we therefore use a range of accelerations from 100 to 500 m/s² in our calculations.

We compute the accelerational forces acting on algae from Eq. 6 using accelerations of 100, 250, or 500 m/s², species-mean $C_{m,\mathrm{avg}}$ values (from Table 2), and volume expressed as a function of area (via the appropriate relation of Table 6). Note that although the $C_{m,\mathrm{avg}}$'s used in the calculations were measured at peak accelerations of only 0.8 m/s² (two orders of magnitude smaller than those expected in the surf zone), hydrodynamic theory for inviscid fluids predicts the inertia coefficient to be independent of acceleration magnitude. While experimental data from real flows show this to be an idealization, the inertia coefficient appears to depend on acceleration magnitude only secondarily and only under particular flow conditions (Sarpkaya and Tuter 1974). Thus we feel justified in using the $C_{m,\mathrm{avg}}$ values determined using the oscillating-flow tank to estimate the accelerational forces acting on algae in the field. These accelerational forces are then added to the drag forces discussed earlier to arrive at estimates of the maximal total in-line forces impinging on algae of given size during given time intervals.

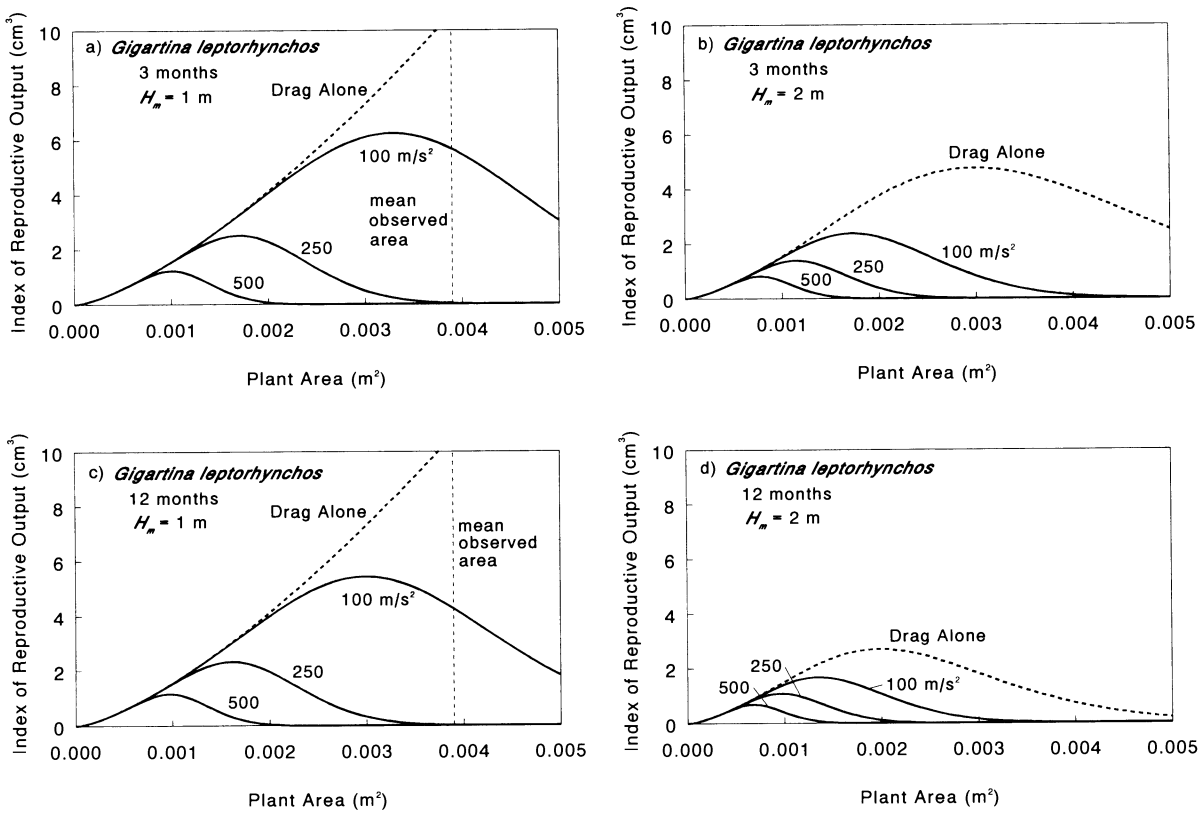

FIG. 14. Index of reproductive output for a period of 3 and 12 mo for *Gigartina leptorhynchos* growing at sites of two different exposures. Solid lines are predictions based on drag plus accelerations of 100, 250, or 500 m/s². The mean observed area for this species is shown in panels where conditions match those expected for the site where these plants were collected (H_m = 1 m, a = 100 m/s²). (a) H_m = 1 m, 3 mo. (b) H_m = 2 m, 3 mo. (c) H_m = 1 m, 12 mo. (d) H_m = 2 m, 12 mo.

The effects of the accelerational force are notable. The probability of survival is substantially decreased by the presence of the accelerational force (Fig. 13) and the size of predicted maximal reproductive output is concomitantly reduced (Figs. 14–16). The optimal sizes predicted on the basis of a total force composed of both drag and the accelerational force are much closer to the sizes actually observed than those predicted for drag alone.

The optimal size predicted by our calculations is relatively insensitive to the period of time considered. This is due to the fact that maximal drag (which in our calculation is a function of time) forms a small fraction of the net force, while the accelerational force (which we have modeled as independent of time) accounts for most of the total force. Estimates of optimal size are sensitive, however, to the waviness of the sea: larger optimal sizes are predicted for sites with a lower mean significant wave height.

For *G. leptorhynchos*, collected at the more protected of our sites, the predictions based on H_m = 1 m closely approximate plant size if a = 100 m/s², an acceleration magnitude that might be expected for typical flow conditions and plant sizes at this location (Denny et al. 1985). In particular, the predicted optimal sizes for *G. leptorhynchos* for 12 and 3 mo are 0.0030 and 0.0033 m², respectively, quite near the mean observed area of 0.0039 m² (Fig. 14). The model also suggests that at an exposed site (H_m = 2 m) *G. leptorhynchos* individuals, if present, should be only one-third to one-half the size observed at our moderately exposed collection site, but we have not tested this prediction.

For *P. limitata* and *I. flaccida* (collected at an exposed site), A_{opt} is more closely predicted when a = 250 m/s². For example, the predicted optimal sizes for *P. limitata* for 12 and 3 mo are 0.0033 and 0.0036 m², respectively, almost identical to the mean observed A of 0.0034 m² (Fig. 15). Similarly, A_{opt} for *I. flaccida* over 12 and 3 mo is 0.0072 and 0.0078 m², again close to the observed size (mean A = 0.0083 m², Fig. 16). This is consistent with the expectation that larger accelerations are present at more exposed locations.

Since we have not directly measured accelerations at our sites, these calculations of A_{opt} must be viewed as preliminary. Nevertheless, the correspondence of the predicted optimal sizes to the mean observed sizes suggests that hydrodynamic forces may indeed be an important agent constraining size in these species.

Avoiding large accelerations.—*G. leptorhynchos, P. limitata,* and *I. flaccida* are substantially smaller than

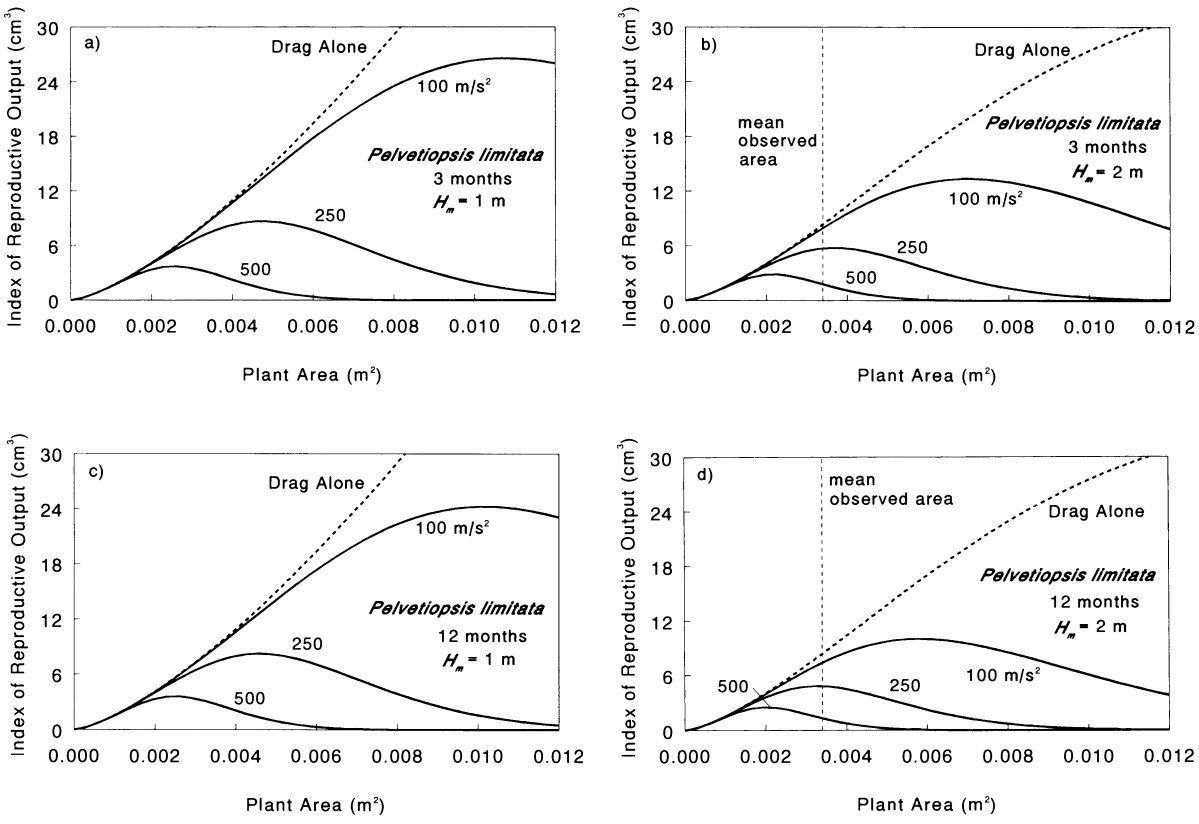

FIG. 15. Index of reproductive output for a period of 3 and 12 mo for *Pelvetiopsis limitata* growing at sites of two different exposures. Solid lines are predictions based on drag plus accelerations of 100, 250, or 500 m/s². The mean observed area for this species is shown in panels where conditions match those expected for the site where these plants were collected (H_m = 2 m, a = 250 m/s²). (a) H_m = 1 m, 3 mo. (b) H_m = 2 m, 3 mo. (c) H_m = 1 m, 12 mo. (d) H_m = 2 m, 12 mo.

a number of other marine plants (e.g., *Egregia menziesii, Macrocystis pyrifera,* and *Nereocystis luetkeana*). However, the existence of these larger organisms does not necessarily contradict the model presented above. There are several strategies that may allow algae to reach sizes larger than those typical of the species tested here.

For instance, *Egregia,* the feather-boa kelp, has a strap-like frond with relatively little thallus area per stipe cross-sectional area and a sturdy perennial holdfast. Since mechanical constraints on size for a given species are determined by that organism's allometric pattern of growth and its strength distribution, it seems likely that this plant attains its large size by being exceptionally strong.

A second strategy is exemplified by *Macrocystis* and *Nereocystis,* both of which grow from holdfasts typically located at depths of 6–20 m. Wave-induced flows at these depths are benign compared to those in the surf zone (Denny 1988). As a result, juvenile *Macrocystis* and *Nereocystis* may grow to lengths of several metres before they encounter the violent flows characteristic of surface waters. Their length may then allow them to "go with the flow" (sensu Koehl 1984), reducing the drag they must withstand. Furthermore, accelerations in nonbreaking waves are 1–2 orders of magnitude smaller than those in the surf zone, greatly relaxing any size constraints imposed by the accelerational force (it is interesting to note that kelp forests are usually located just offshore of where waves begin to break [Seymour et al. 1989]). Thus these algae apparently avoid the effects of large accelerations by taking advantage of spatial gradients in flow severity.

Theoretically, the consequences of severe wave action can also be avoided by taking advantage of temporal differences in wave exposure. If, during a seasonal lull in wave action, a plant can grow long enough to effectively "go with the flow," it may attain a refuge in size from the mechanical constraints discussed here. Although this strategem may be possible in theory, we know of no clear case in which it appears to operate in nature. Many species of intertidal algae grow large in the summer months when wave heights are relatively small, but none on our local shores appear to attain lengths sufficient to escape the destructive effects of water motion, and the first few winter storms effectively dislodge or prune the plants.

An alga's material properties as well as thallus shape

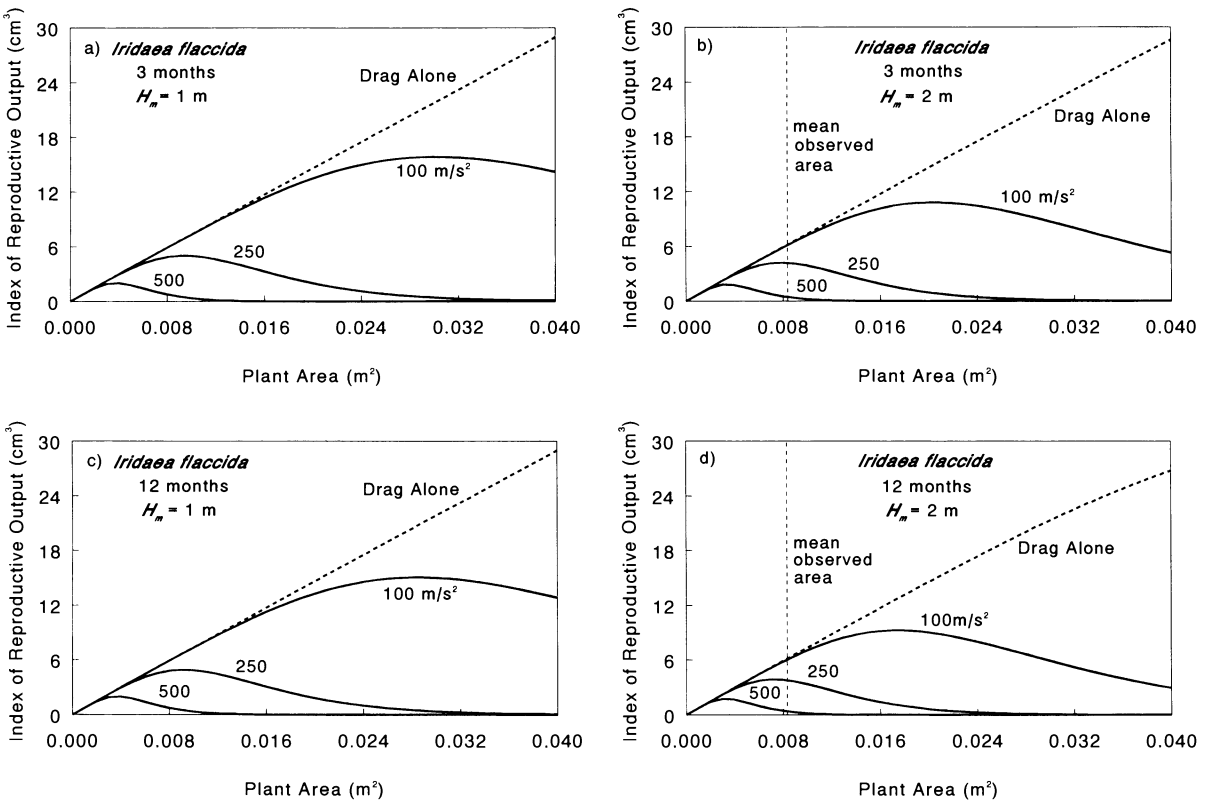

FIG. 16. Index of reproductive output for a period of 3 and 12 mo for *Iridaea flaccida* growing at sites of two different exposures. Solid lines are predictions based on drag plus accelerations of 100, 250, or 500 m/s². The mean observed area for this species is shown in panels where conditions match those expected for the site where these plants were collected (H_m = 2 m, a = 250 m/s²). (a) H_m = 1 m, 3 mo. (b) H_m = 2 m, 3 mo. (c) H_m = 1 m, 12 mo. (d) H_m = 2 m, 12 mo.

determine how it will respond to mechanical stresses. In general, macroalgae have low stiffness and strength and high extensibility when compared to many other biomaterials (Koehl and Wainwright 1977, Koehl 1986, Denny et al. 1989). This high degree of flexibility and extensibility provides shock absorption that may reduce the stresses induced by transient dynamic loads, allowing intertidal algae to more easily sustain the short pulses of rapid water motion characteristic of wave-swept rocky shores (Koehl 1984, Denny 1987*b*). Note that such structural compliance cannot reduce the effective magnitude of constant or near-constant forces, but only those that change relatively rapidly through time. Thus while the "stretchiness" of algae may, for example, allow them to survive large, but exceptionally brief accelerations (such as the 1000–2000 m/s² accelerations postulated by Denny et al. [1985] to accompany winter storms), the 500 m/s² accelerations actually measured by Denny et al. are likely to be of sufficient duration that dynamic effects become relatively unimportant. In general, the utility of algal extensibility as a mechanism for reducing the effective strength of hydrodynamic forces remains unclear, since neither the magnitude nor duration of surf-zone accelerations has been described in any detail.

The reality of algal accelerational forces: a critical examination

Reorientation in oscillatory flow.—The methods used in this study to predict the hydrodynamic forces acting on organisms rely at their most basic level on developing a description of drag and inertia coefficients typical of a given species. The greatest difficulty in determining C_d's and $C_{m,\text{avg}}$'s of algae in unsteady flow results from the variation in algal shape as velocities and accelerations change. All of the plants tested in this study moved and reoriented with flow during a small fraction of each cycle. The effect of this behavior on algal drag coefficients is relatively well understood: C_d's decline with increasing velocity due to reconfiguration (thallus compression). However, the effect of such movement on the inertia coefficient is less clear. In harmonic flow, peak accelerations occur at times of zero velocity, which correspond to the brief instants when the plants swing from an upstream orientation to one where they lay extended downstream, that is, when they are moving with the fluid. Although the precise consequences of this behavior are difficult to ascertain, a tentative answer to this question is provided from tests using the tethered perforated hollow sphere.

By allowing the perforated sphere to travel a short distance with the flow, the tether of this model provides an analogue to the ability of a flexible organism to reorient. The effects of such movement were compared to the data for the same shape, rigidly mounted. The average inertia coefficient for the tethered perforated sphere was 2.6, as compared to 7.6 for the immobile perforated sphere (Table 2). Evidently, going with the flow can reduce, but need not eliminate, the effects of accelerational forces in reorienting objects.

Potential artifacts in the analysis.—The procedure used in this study to determine C_d and $C_{m,\mathrm{avg}}$ relies on separating the total in-line force into its respective sine and cosine components, using the assumption that the sum of the odd sine terms represents drag while the cosine term represents the accelerational force. There is, however, a potential complication with this method that we have not yet addressed.

The sum of a sine and a cosine term can also be expressed simply as a sine term with a phase shift. This implies that the cosinusoidal forces we recorded are potentially just a consequence of drag that has somehow been shifted in time. For example, drag could mimic the accelerational component in our force records if the cycle of drag preceded the cycle of velocity. However, there is no obvious means by which drag forces could be phase shifted for stationary, inflexible objects, and a reorienting object that moves with the fluid is unlikely to have peak drag forces that lead peak velocities.

This last point may be clarified by examining how the cycle of drag could theoretically lead velocity (that is, how drag could begin to decline even as velocity increases). We consider two possible scenarios.

First, an alga might reorient only in response to a rather large force, but then after swinging around to its new position, lay down in the boundary layer where velocities are lower. Although this might indeed produce a force trace that would peak prior to the mainstream velocity, such behavior is implausible in the oscillating-flow tank where the turbulent boundary layer is quite thin (see *Materials and methods: Measurements in unsteady flow*) and where major portions of algal thallus mass remain from 1 to 3 cm from the wall (entirely outside the boundary layer), even in rapid flow.

A second possible means by which the cycle of drag could precede that of velocity is supplied by a C_d that drops so steeply with increasing flow rate that its decline outpaces the effects of the higher velocity itself. This is equivalent to saying that reconfiguration, which occurs in response to drag, would somehow have to act so as to reduce the drag force that is in fact its proximal cause. Not only does this appear unlikely on physical grounds, but from a mathematical perspective it can be shown that this would require an E value more negative than -2.0, whereas the most negative E value we measured was -1.01 (Table 4).

Thus, although all that is required in theory for drag to mimic acceleration in our experiments is that the cycle of drag force precede that of velocity, in practice the physical means by which this could occur can be discounted as unlikely. Note that the converse situation (misrepresenting accelerational forces as drag) is of lesser concern since the drag signal is substantially larger than the accelerational signal in our experiments, and any small accelerational force mistakenly identified as drag would therefore have only minor impact on calculations of C_d. While an accelerational force inappropriately attributed to drag would also produce a smaller estimate of $C_{m,\mathrm{avg}}$, the potential for such an effect simply means that the values we have used in our calculations are conservative.

Limitations of the approach: variable C_m.—The changes in algal shape associated with reorientation and reconfiguration also produce drag and inertia coefficients that vary through the course of an oscillatory cycle. We have previously described the manner in which C_d changes with velocity. However, quantifying the variation in C_m is more difficult due to the small magnitude of the accelerational force as compared to the size of the drag force (Fig. 7, Table 2). This small accelerational force "signal" renders estimates of the variation of C_m during a cycle sensitive to turbulent fluctuations in flow and electronic noise in the recording apparatus. As a result, only average C_m values were computed in the analysis.

However, ignoring higher order variation may, at times, produce misleading results. For example, while negative instantaneous C_m values are entirely possible (see the Appendix), negative average inertia coefficients are unlikely. On this basis we propose that the negative $C_{m,\mathrm{avg}}$ value for the first run of the second sample of *I. flaccida* (Table 2) is anomalous and may be an artifact of using only the first cosine harmonic in its estimation. The low $C_{m,\mathrm{avg}}$ for this run may result from the fact that the third cosine harmonic, which was discarded with the rest of the higher order terms, was much larger than the primary cosine harmonic. Thus, in this case, by ignoring the higher harmonics, much of the information regarding the accelerational force acting on the alga was lost. This experimental trial was unique in this regard.

Other factors affecting plant size.—While no organism can grow larger than physics will allow, in some cases biological factors place more stringent constraints on size than those set by mechanical factors. The model developed above considers only strength distributions, basic morphology, and wave exposure in predicting optimal size. Furthermore, we have chosen to represent fecundity in perhaps the simplest manner possible (via volume). These simplifications, while enhancing model utility, also eliminate from consideration factors that are often important in determining algal size. As such, the model used in this study is not universally appropriate. We briefly note some of the more obvious fac-

tors that could reduce the applicability or efficacy of this approach.

First, regardless of an alga's material properties, a plant can be dislodged if the adhesion of its holdfast to the substratum fails. Some seaweeds such as *Postelsia palmaeformis* are detached when the rock, mussel, alga, or barnacle to which they are attached breaks free or dies (Dayton 1973, Paine 1979). In this case, characteristics of the substrate may determine the maximal force an alga can survive and thereby may constrain its size.

Seaweeds also possess a great capacity to modify their shape and size to suit conditions that can vary considerably throughout the plant's lifetime (Norton et al. 1981). Perennial algae have meristems that remain totipotent, tailoring plant form to prevailing conditions (Norton 1991). This morphological plasticity means that individuals of the same species (or even genotype) can appear quite different. Such differences in form can potentially alter the force an alga of a given thallus area will feel at a particular velocity and acceleration and might therefore shift its optimal size.

Seasonal variation in the severity of wave action can also affect plant size. While an alga may grow beyond the yearly optimum during an extended calm period (i.e., summer), it is likely to be either disloged or pruned back to a more sustainable size in a subsequent storm. Since many algae perennate (regrow from a permanent holdfast), growth to a size beyond the yearly optimum provides a means for an alga to "take a chance" and reach an even larger size, achieving a correspondingly greater reproductive output (B. Menge, *personal communication*). On the one hand, if no storm arrives before the time of reproduction, the alga will have an exceptionally successful season. If on the other hand a storm does arrive, often only a portion of the alga will be torn off, reducing its overall size but not destroying it. In this case, even if the alga is completely pruned back to holdfast alone, it remains capable of growing in the future, and can sometimes even regenerate enough body tissue to elicit a modest bout of reproduction within the same season.

Note also that large size may not always be advantageous. In our arguments here we have equated large size with increased reproductive output, but have not taken into account the time it takes to grow. It is possible that a plant could increase the relative rate at which its genes are contributed to the species gene pool by growing rapidly to a small size, reproducing, and growing again. Such a life history strategy argues for determinate growth in algae, and could result in plants of a size smaller than the optimum predicted using this model.

Vegetative propagation serves as an important reproductive strategy in seaweeds (Cheney and Mathieson 1978). In particular, vegetative propagation via fragmentation may be a useful mechanism of asexual reproduction and spore dispersal. Broken-off tissue may contain spores, conceptacles, or gametes or may be able to reattach to the substratum and grow (Norton et al. 1982). Since algal materials often have a low work of fracture (Denny et al. 1989), a plant with nicks or surface flaws can easily lose branches or portions of blades even at forces too weak to endanger the thallus as a whole. In combination with perennation, such nonlethal pruning might account for much of an alga's reproductive success. This possibility has been ignored in our predictions of optimal size.

In general, the success of a plant in a particular environment can only be fully understood in the context of its physiology, reproductive biology, and ecological role. Hydrodynamic forces and their consequences for survival are only one in a complex suite of factors that determine the size of intertidal algae. Grazing, nutrient supply, "tattering" or other nonlethal pruning of plants, heat stress and desiccation, crowding and light availability, as well as other factors, can all affect plant size. As such, the "appropriate" plant form will be site specific since intertidal areas differ in the conditions they impose and the resources they supply.

The presence of biological constraints on the maximal size of wave-swept algae does not, however, detract from the utility of the mechanical approach proposed here. Indeed, although the results of this study must be considered preliminary, the predicted optimal sizes are nevertheless tantalizingly close to the actual sizes of plants observed in the field. While we hesitate to suggest without further data that hydrodynamic forces might in general be a primary factor constraining the size of intertidal organisms, we emphasize that the potential for wave forces to act as a widespread limit to size exists. This suggests that attention solely to biological factors (without exploring their linkage to mechanical parameters) is ill advised and that research further examining the role of wave action in setting size limits in the intertidal zone is both warranted and important.

Acknowledgments

We thank T. L. Daniel, M. A. R. Koehl, B. Menge, and E. Carrington Bell for helpful comments on the manuscript and J. Harding for lending his artistic talents to the illustrations. Funds for this study were provided by the National Science Foundation (grant OCE-9115688 to M. W. Denny), the Office of Naval Research (contract N00014-87-K-0685-A00003 to M. W. Denny), the Myers Oceanographic and Marine Biology Trust to B. Gaylord, and the Phycological Society of America Croasdale Fellowship to C. Blanchette.

Literature Cited

Abbott, I. A., and G. J. Hollenberg. 1976. Marine algae of California. Stanford University Press, Stanford, California, USA.

Armstrong, S. L. 1984. Functional morphology and tissue mechanics of the brown alga *Hedophyllum sessile*. Dissertation. Duke University, Durham, North Carolina, USA.

Batchelor, G. K. 1967. An introduction to fluid dynamics. Cambridge University Press, Cambridge, England.

Caceci, M. S., and W. P. Cacheris. 1984. Fitting curves to data. BYTE **9**:340–362.

Carrington, E. 1990. Drag and dislodgment of an intertidal macroalga: consequences of morphological variation in *Mastocarpus papillatus* Kützing. Journal of Experimental Marine Biology and Ecology **139**:185–200.

Charters, A. C., M. Neushul, and C. Barilotti. 1969. The functional morphology of *Eisenia arborea*. Proceedings of the International Seaweed Symposium **6**:89–105.

Cheney, D. P., and A. C. Mathieson. 1978. On the ecological and evolutionary significance of vegetative propagation in seaweeds. Journal of Phycology **14**:27.

Dayton, P. K. 1971. Competition, disturbance, and community organization: the provision and subsequent utilization of space in a rocky intertidal community. Ecological Monographs **41**:351–389.

———. 1973. Dispersion, dispersal and persistence of the annual intertidal alga, *Postelsia palmaeformis* Ruprecht. Ecology **54**:433–438.

Denny, M. W. 1987*a*. Lift as a mechanism of patch initiation in mussel beds. Journal of Experimental Marine Biology and Ecology **113**:231–245.

———. 1987*b*. Life in the maelstrom: the biomechanics of wave-swept rocky shores. Trends in Ecology and Evolution **2**:61–66.

———. 1988. Biology and the mechanics of the wave-swept environment. Princeton University Press, Princeton, New Jersey, USA.

———. 1989. A limpet shell shape that reduces drag: laboratory demonstration of a hydrodynamic mechanism and an exploration of its effectiveness in nature. Canadian Journal of Zoology **67**:2098–2106.

———. 1991. Biology, natural selection and the prediction of maximal wave-induced forces. South African Journal of Marine Science **10**:353–363.

———. 1993. Disturbance, natural selection and the prediction of maximal wave induced forces. Contemporary Mathematics **141**:65–90.

Denny, M. W., V. Brown, E. Carrington, G. Kraemer, and A. Miller. 1989. Fracture mechanics and the survival of wave-swept macroalgae. Journal of Experimental Marine Biology and Ecology **127**:211–228.

Denny, M. W., T. L. Daniel, and M. A. R. Koehl. 1985. Mechanical limits to size in wave-swept organisms. Ecological Monographs **55**:69–102.

Denny, M. W., and S. D. Gaines. 1990. On the prediction of maximal intertidal wave forces. Limnology and Oceanography **35**:1–15.

Fox, R. W., and A. T. McDonald. 1985. Introduction to fluid mechanics. John Wiley & Sons, New York, New York, USA.

Gaines, S. D., and M. W. Denny. 1993. The largest, smallest, highest, lowest, longest, and shortest: extremes in ecology. Ecology **74**:1677–1692.

Hoerner, S. F. 1965. Fluid-dynamic drag. Published by the author, Brick Town, New Jersey, USA.

Jones, W. E., and A. Demetropoulos. 1968. Exposure to wave action: measurements of an important ecological parameter on rocky shores on Anglesey. Journal of Experimental Marine Biology and Ecology **2**:46–63.

Koehl, M. A. R. 1977*a*. Effects of sea anemones on the flow forces they encounter. Journal of Experimental Biology **69**: 87–105.

———. 1977*b*. Mechanical diversity of connective tissue of the body wall of sea anemones. Journal of Experimental Biology **69**:107–125.

———. 1977*c*. Mechanical organization of cantilever-like sessile organisms: sea anemones. Journal of Experimental Biology **69**:127–142.

———. 1984. How do benthic organisms withstand moving water? American Zoologist **24**:57–70.

———. 1986. Seaweeds in moving water: form and mechanical function. Pages 603–634 *in* T. J. Givnish, editor. On the economy of plant form and function. Cambridge University Press, Cambridge, England.

Koehl, M. A. R., and R. S. Alberte. 1988. Flow, flapping, and photosynthesis of *Nereocystis luetkeana*: a functional comparison of undulate and flat blade morphologies. Marine Biology **99**:435–444.

Koehl, M. A. R., and S. A. Wainwright. 1977. Mechanical adaptations of a giant kelp. Limnology and Oceanography **22**:1067–1071.

Leigh, E. G., R. T. Paine, J. F. Quinn, and T. H. Suchanek. 1987. Wave energy and intertidal productivity. Proceedings of the National Academy of Sciences (USA) **84**:1314–1318.

Massey, B. S. 1989. Mechanics of fluids. Sixth edition. Van Nostrand Reinhold (International), London, England.

Middleton, G. V., and J. B. Southard. 1984. Mechanics of sediment movement. Society of Economic Paleontologists and Mineralogists, Tulsa, Oklahoma, USA.

Norton, T. A. 1991. Conflicting constraints on the form of intertidal algae. British Phycological Journal **26**:203–218.

Norton, T. A., A. C. Mathieson, and M. Neushul. 1981. Morphology and environment. Pages 421–451 *in* C. S. Lobban and M. J. Wynne, editors. The biology of seaweeds. Blackwell Scientific, Oxford, England.

Norton, T. A., A. C. Mathieson, and M. Neushul. 1982. A review of some aspects of form and function in seaweeds. Botanica Marina **25**:501–510.

Paine, R. T. 1979. Disaster, catastrophe, and the local persistence of the sea palm, *Postelsia palmaeformis*. Science **205**:685–687.

Paine, R. T., and S. A. Levin. 1981. Intertidal landscapes: disturbance and the dynamics of pattern. Ecological Monographs **51**:145–178.

Sarpkaya, T. 1976. Forces on cylinders near a plane boundary in a sinusoidally oscillating fluid. Transactions of the American Society of Mechanical Engineers Journal of Fluids Engineering **98**:499–505.

Sarpkaya, T., and M. Isaacson. 1981. Mechanics of wave forces on offshore structures. Van Nostrand Reinhold, New York, New York, USA.

Sarpkaya, T., and O. Tuter. 1974. Forces on cylinders and spheres in a sinusoidally oscillating fluid. Naval Postgraduate School Technical Report NPS-59SL74091. Naval Postgraduate School, Monterey, California, USA.

Schlichting, H. 1979. Boundary-layer theory. Seventh edition. McGraw-Hill, New York, New York, USA.

Seymour, R. J., M. J. Tegner, P. K. Dayton, and P. E. Parnell. 1989. Storm wave induced mortality of giant kelp, *Macrocystis pyrifera*, in southern California. Estuarine, Coastal and Shelf Science **28**:277–292.

Sheath, R. G., and J. A. Hambrook. 1988. Mechanical adaptations to flow in freshwater red algae. Journal of Phycology **24**:107–111.

Sousa, W. P. 1984. The role of disturbance in natural communities. Annual Review of Ecology and Systematics **15**: 353–391.

———. 1985. Disturbance and patch dynamics on rocky intertidal shores. Pages 101–124 *in* S. T. A. Pickett and P. S. White, editors. The ecology of natural disturbance and patch dynamics. Academic Press, New York, New York, USA.

Stephenson, T. A., and A. Stephenson. 1949. The universal features of zonation between tide-marks on rocky coasts. Journal of Ecology **37**:289–305.

Vogel, S. 1981. Life in moving fluids. Princeton University Press, Princeton, New Jersey, USA.

———. 1984. Drag and flexibility in sessile organisms. American Zoologist **24**:37–44.

———. 1989. Drag and reconfiguration of broad leaves in high winds. Journal of Experimental Botany **40**:941–948.

APPENDIX

Negative Instantaneous C_m

The accelerational force acting on a stationary object in an accelerating fluid can be viewed as the rate of change of momentum of the fluid–object system over and above that occurring in steady flow. This can be expressed as $d(mu)/dt$, where m is the mass of the system and t is time. When the mass, m, remains constant, the change in momentum equals mdu/dt, where du/dt is the fluid's acceleration. This produces the familiar form of Newton's Second Law: $F = ma$. However, when the mass changes with time, the accelerational force must be expressed as $d(mu)/dt$. Here, we have a "mass" that equals $(\rho V + C_a\rho V)$. Thus,

$$F_a = d[(\rho V + C_a\rho V)u]/dt.$$

For an object with constant volume but variable added mass (e.g., an object whose orientation or shape changes with time) and for a fluid with constant density:

$$\begin{aligned} F_a &= \rho V d[(1 + C_a)u]/dt \\ &= \rho V(du/dt + udC_a/dt + C_a du/dt). \end{aligned}$$

Thus, the rate of change of C_a (represented by dC_a/dt) can affect the accelerational force, as well as the absolute magnitude of the added mass coefficient. Substituting into the equation,

$$F_a = C_m\rho Va,$$

and rearranging yields the following expression for C_m:

$$\begin{aligned} C_m &= 1 + (udC_a/dt)/(du/dt) + C_a \\ &= 1 + udC_a/du + C_a. \end{aligned}$$

Thus for a large enough rate of decrease of C_a (yielding a negative value for the middle term above), C_m can drop below zero. The above expression reduces to the form $(1 + C_a)$ for a constant added mass or inertia coefficient, the form used in the present study.